Acta Biomaterialia 156 (2023) 88–109

Contents lists available at ScienceDirect

Acta Biomaterialia

journal homepage: www.elsevier.com/locate/actbio

Review article

Unveiling the potential of melt electrowriting in regenerative dental medicine☆

Arwa Daghrery[a,b], Isaac J. de Souza Araújo[a], Miguel Castilho[c,d,e], Jos Malda[c,d,f,*], Marco C. Bottino[a,g,**]

[a] Department of Cardiology, Restorative Sciences, and Endodontics, University of Michigan, School of Dentistry, Ann Arbor, Michigan, United States
[b] Department of Restorative Dental Sciences, School of Dentistry, Jazan University, Jazan, Saudi Arabia
[c] Regenerative Medicine Center, University Medical Center Utrecht, Utrecht, the Netherlands
[d] Department of Orthopedics, University Medical Center Utrecht, Utrecht, the Netherlands
[e] Department of Biomedical Engineering, Eindhoven University of Technology, Eindhoven, the Netherlands
[f] Department of Clinical Sciences, Faculty of Veterinary Medicine, Utrecht University, Utrecht, the Netherlands
[g] Department of Biomedical Engineering, College of Engineering, University of Michigan, Ann Arbor, Michigan, United States

ARTICLE INFO

Article history:
Received 3 September 2021
Revised 8 December 2021
Accepted 5 January 2022
Available online 10 January 2022

Keywords:
Melt electrowriting
3D printing
Biofabrication
Dentistry
Regeneration
Scaffolds

ABSTRACT

For nearly three decades, tissue engineering strategies have been leveraged to devise effective therapeutics for dental, oral, and craniofacial (DOC) regenerative medicine and treat permanent deformities caused by many debilitating health conditions. In this regard, additive manufacturing (AM) allows the fabrication of personalized scaffolds that have the potential to recapitulate native tissue morphology and biomechanics through the utilization of several 3D printing techniques. Among these, melt electrowriting (MEW) is a versatile direct electrowriting process that permits the development of well-organized fibrous constructs with fiber resolutions ranging from micron to nanoscale. Indeed, MEW offers great prospects for the fabrication of scaffolds mimicking tissue specificity, healthy and pathophysiological microenvironments, personalized multi-scale transitions, and functional interfaces for tissue regeneration in medicine and dentistry. Excitingly, recent work has demonstrated the potential of converging MEW with other AM technologies and/or cell-laden scaffold fabrication (bioprinting) as a favorable route to overcome some of the limitations of MEW for DOC tissue regeneration. In particular, such convergency fabrication strategy has opened great promise in terms of supporting multi-tissue compartmentalization and predetermined cell commitment. In this review, we offer a critical appraisal on the latest advances in MEW and its convergence with other biofabrication technologies for DOC tissue regeneration. We first present the engineering principles of MEW and the most relevant design aspects for transition from flat to more anatomically relevant 3D structures while printing highly-ordered constructs. Secondly, we provide a thorough assessment of contemporary achievements using MEW scaffolds to study and guide soft and hard tissue regeneration, and draw a parallel on how to extrapolate proven concepts for applications in DOC tissue regeneration. Finally, we offer a combined engineering/clinical perspective on the fabrication of hierarchically organized MEW scaffold architectures and the future translational potential of site-specific, single-step scaffold fabrication to address tissue and tissue interfaces in dental, oral, and craniofacial regenerative medicine.

Statement of significance

Melt electrowriting (MEW) techniques can further replicate the complexity of native tissues and could be the foundation for novel personalized (defect-specific) and tissue-specific clinical approaches in regenerative dental medicine. This work presents a unique perspective on how MEW has been translated towards the application of highly-ordered personalized multi-scale and functional interfaces for tissue re-

☆ Part of the Special Issue on Biofabrication for Orthopedic, Maxillofacial, and Dental Applications, guest-edited by Professors Hala Zreiqat, Khoon Lim, and Debby Gawlitta

* Corresponding author at: University Medical Center Utrecht, Huispostnummer: G05.228, Postbus 85500, 3508 AB Utrecht, the Netherlands.
** Corresponding author at: University of Michigan, School of Dentistry, Department of Cariology, Restorative Sciences, and Endodontics, 1011 N University (Room 5223), Ann Arbor, MI 48109, United States.
E-mail addresses: j.malda@umcutrecht.nl (J. Malda), mbottino@umich.edu (M.C. Bottino).

https://doi.org/10.1016/j.actbio.2022.01.010

generation, targeting the transition from flat to anatomically-relevant three-dimensional structures. Furthermore, we address the value of convergence of biofabrication technologies to overcome the traditional manufacturing limitations provided by multi-tissue complexity. Taken together, this work offers abundant engineering and clinical perspectives on the fabrication of hierarchically MEW architectures aiming towards site-specific implants to address complex tissue damage in regenerative dental medicine.

1. Introduction

Numerous health conditions, such as cancer, severe trauma, congenital deformity, and progressive destructive diseases, may compromise and damage the function of complex tissues in the craniofacial region, including bone, cartilage, and soft tissues, leading to irreparable deformities [1–3]. As a result, a plethora of reconstructive therapies has been portrayed in the literature since the inception of the field of tissue engineering [4]. However, these reconstructions primarily focus on repairing bone defects using grafts from either autologous, homologous, or heterologous sources [3]. Despite the osteoinductive outcomes achieved with these graft options, the need for two surgical areas, the extended morbidity for autologous grafts and the variable results from the allogenic and xenogeneic grafts [5], continue to pose significant clinical concerns. Therefore, to overcome the shortcomings of traditional reconstructive techniques, proven concepts of tissue engineering have provided solid direction for clinical translation of innovative technologies and therapeutics. Countless approaches have been proposed to develop safe and effective therapies for dental, oral, and craniofacial (DOC) tissue regeneration **(Fig. 1)**. In essence, methods involving the utilization of scaffolds, biomolecules (*e.g.*, growth factors), and/or cells have been offered to repair or regenerate DOC tissues [3]. To that end, a range of biomaterials, including polymers (natural and synthetic), ceramics and composites have been used in the fabrication of scaffolds, *i.e.*, matrices to facilitate the migration, support or transport of cells and/or biomolecules to encourage tissue neoformation.

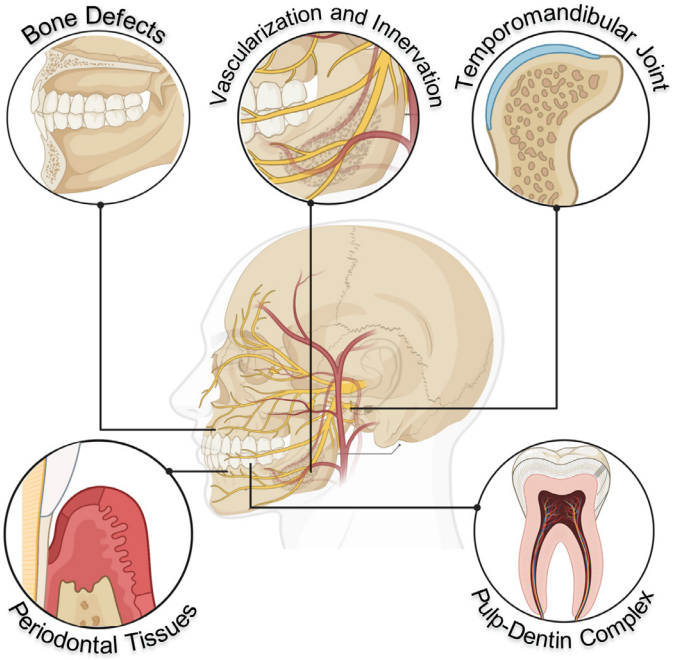

Fig. 1. Schematic illustration of the anatomy of relevant dental, oral, and craniofacial (DOC) tissues; craniomaxillofacial bone and periodontal complex (*i.e.*, alveolar bone, gingiva, periodontal ligament [PDL], and cementum).

Since its establishment, the field of regenerative medicine has stimulated considerable advances in the creation of biomimetic scaffold templates of the extracellular matrix (ECM) through several methods, including, but not limited to, electrospinning, thermally-induced phase separation, and solvent casting and particulate leaching [3]. Amongst these, solution-based electrospinning has been one of the most used techniques due to its versatile, facile, and reasonably inexpensive fabrication technology [6,7]. However, the lack of control over fiber deposition typically results in formation of densely-packed sheet-like fibrous structures that limit cellular infiltration and vascularization [6–8]. As an alternative, additive manufacturing (AM) technologies have emerged as a potential solution to engineering scaffolds with controlled architectures that can better replicate the complex 3D organization of human tissues. For instance, fused deposition modeling (FDM), a technique based on the selective dispensing of a molten polymer through a nozzle, allows for the generation of mechanically-competent 3D scaffolds and implants [9]. Recently, aiming at the fabrication of 3D scaffolds and implants that combine conflicting properties such as mechanical performance and high porosity, the concept of digital design via optimization techniques or parametric design has been coupled with AM technologies [10–14]. Unfortunately, while FDM-processed scaffolds can be modified with bioceramics to afford better biological properties, for example in bone tissue engineering [9,15,16], these scaffolds present low spatial resolution, and morphological features that are several orders of magnitude larger than native ECM [7,17]. Thus, intending to circumvent the low resolution of scaffolds processed via FDM and the poor organization of electrospun alternatives, the principles of thermal polymer extrusion and electrospinning have been combined in a process coined Melt Electrospinning Writing, or simply Melt ElectroWriting (MEW) [17,18].

MEW consists of the application of an electrical field to draw a molten polymer continuously out of a spinneret towards a computer controlled planar or rotating collector plate **(Fig. 2A-B)** [19–21]. The collector plate translates at a speed close to that of the jet, which allows for highly-ordered fiber deposition and stacking to create 3D scaffolds and architectures [18]. Hitherto, MEW has demonstrated to be a promising enabling tool in regenerative medicine, capable of generating highly-ordered porous structures with fiber filaments ranging from a few hundred nanometers to several microns [18,22–24]. This 3D printing technology is distinct from others in that the outstanding fiber diameter resolution (nano/micrometer) is accompanied with the capability to print one-centimeter thick 3D structures [6,23,25]. This differs from other extrusion-based 3D printing technologies, like FDM, that have filament diameter resolution limits around 100 μm or are restricted in fabricating macroscale objects. In fact, the highly defined architecture is the reason why MEW structures provide enormous potential for engineering tissue-specific ECM-like scaffolds, pathophysiological microenvironments, personalized and potentially functional implants for DOC tissue regeneration. Additionally, other key aspects relate to recent work on the precise patterning of cell-laden, micron-scale biomaterial fibers [26–28].

Biomaterial-based scaffolds must not only recapitulate the three-dimensional (3D) architecture of the ECM of native tissues,

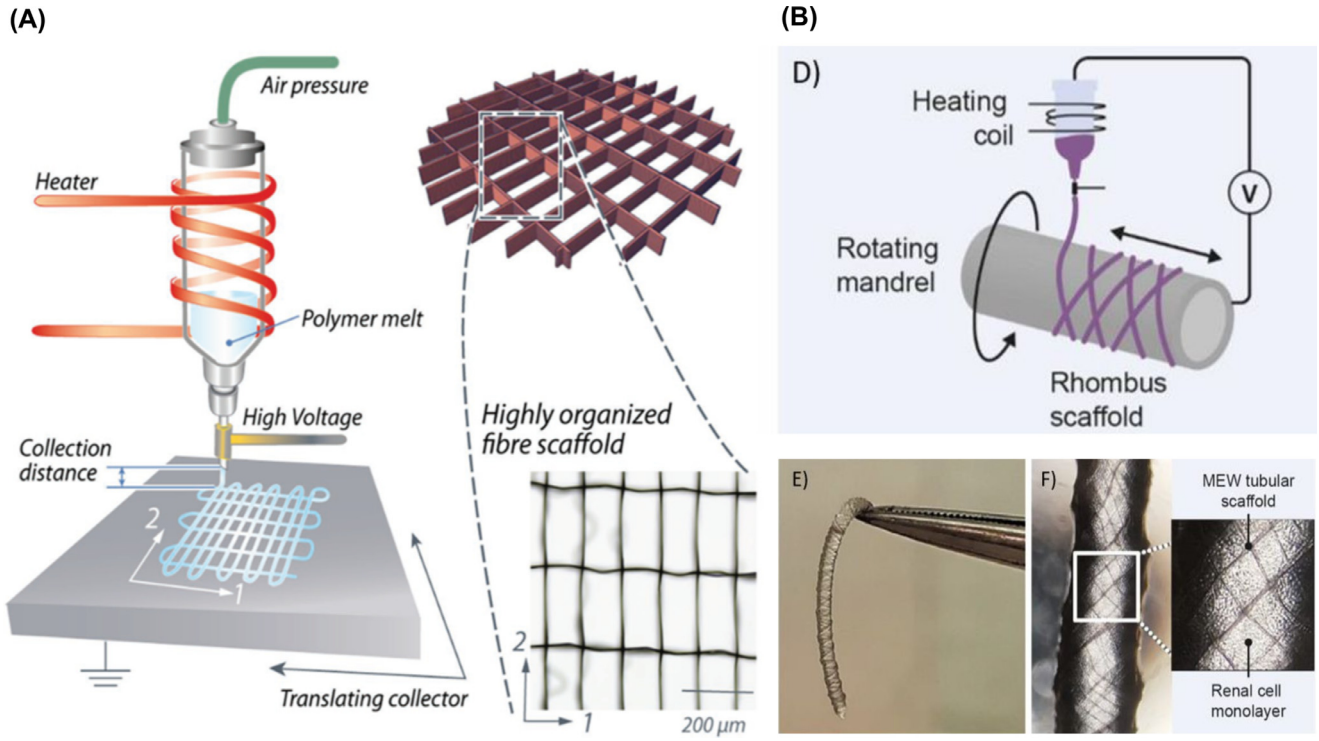

Fig. 2. MEW devices components of air-pressure-assisted dispensing, electrical heating system, and collector at different configurations **(A)** Flat-computer-assisted collector. From Castilho *et al.* (2017) [21]. **(B)** MEW fiber deposition over rotating grounded mandrel to form tubular scaffolds. From Genderen *et al.* (2020) [20].

but also its tissue-specific mechanics and biochemical features for functional tissue regeneration [3]. Here, we offer a brief, yet critical review of the working principles of MEW and the fundamentals involved in the design of tissue- and interface-specific scaffolds for applications in dental, oral, and craniofacial (DOC) regenerative medicine. To the best of our knowledge, we offer a first-hand perspective on its untapped potential in DOC tissue regeneration with an emphasis on the regeneration of mineralized craniofacial tissues, as well as tissue interfaces (*e.g.*, bone-periodontal ligament). As a look forward, we also discuss forthcoming directions related to the utility of MEW as a versatile technology for personalized and functional scaffolds for DOC tissue regeneration and as 3D *in vitro* platform for investigating head and neck tumors.

2. Melt electrowriting – physical principles

To surpass issues regarding fiber orientation and layer organization, in addition to incomplete solvent evaporation commonly associated with solvent-based electrospinning techniques, polymer melts have been used to engineer constructs with controlled fiber diameter, pore size, and 3D architectures. Poly(ε-caprolactone) [PCL] has been the most amenable polymer for MEW, due to its relatively low melting point, semi-crystallinity and rapid solidification, stable thermal and rheological properties, and biocompatibility [29]. Although a range of degradable and non-degradable polymers has been employed to fabricate scaffolds and constructs via MEW, such as polypropylene (PP) [30], a photocurable poly(l-lactide-co-ε-caprolactone-co-acryloyl carbonate) [31], and water-soluble poly(2-ethyl-2-oxazoline) [32], none of them reached (yet) the accuracy of the constructs processed with PCL [33]. Apart from that, to overcome the low elastic properties of PCL, melt-processing of poly(DL-lactide) (PLA)–PCL block copolymers and thermoplastic elastomers (TPE) can be used to develop scaffolds through MEW [33,34].

MEW was conceptualized to achieve better control over small-sized fiber deposition and orientation from polymer melts [29]. The use of a computer controlled moving collector permits accurate deposition of nano- to micron-sized fiber diameters [7]. By moving the collector at speeds matching that of the jet extrusion, the molten polymer can form straight lines in precise patterns that solidify upon polymer cooling [35]. These precisely deposited fibers can be reliably placed on top of each other to repeatedly create 3D structures and personalized scaffolds [18,29], but this requires careful optimization between key material- and instrument-based parameters [36].

Material-based parameters include the molecular weight of the molten polymer, viscosity, and electrical conductivity [37,38]. Meanwhile, instrument-factors encompass the applied electric voltage, collector speed, spinneret diameter, distance from the spinneret to the collector, and extrusion pressure [7,36]. From a material viewpoint highly viscous and low conductivity polymers are considered more stable against sideway paths of polymer jet. Under typical conditions, once the balance between temperature and polymer viscosity has been established, adjusting the aforesaid instrument parameters is key to produce defect-free structures. For instance, increasing pressure increases mass flow; however, high pressure and flow rates for low-viscosity solutions would make it difficult to precisely generate micron-scale and complex 3D arrangements [37].

Moreover, the electrohydrodynamic phenomenon stabilization and continuous flow of polymer melts can be achieved by adjusting the applied voltage and extrusion pressure for direct-writing on the substrate [39]. Insufficient applied electrical force, the main fiber pulling force, leads to the formation of long beads that randomly buckle and largely impair homogeneous fiber deposition, usually defined as pulsing behavior [18,40]. Conversely, higher electrical forces impact on continuous polymer flow and the presence of remnant charges trapped in the polymer fibers, which affects predominantly fiber stacking [35,39]. In addition,

the speed and direction of the collector substrate greatly influence the deposition accuracy.[36] Importantly, to accurately print a highly-ordered scaffold composed of straight fibers, the collector speed must equal the rate of polymer mass flow, *i.e.*, a parameter known by critical translation speed (CTS). At CTS, the shape of the direct-written fiber changes from sinusoidal to a linear morphology [29,39,40]. Although CTS conditions are accepted as ideal to obtain straight fiber scaffolds, research groups, including ours, have shown that complex fiber patterns such as hexagonal shapes, require translation speeds above CTS to accurately allow fiber collection at both straight and corner segments; while other laboratories have demonstrated the potential of printing below CTS to achieve controlled sinusoidal fibrous scaffolds [41]. Collectively, balancing the above-mentioned parameters is essential to achieving well-organized fiber-based MEW scaffolds. The next topic conveys critical information related to design criteria and how they influence the final characteristics of MEW scaffolds and architectures.

3. Designing MEW scaffolds

It is known that the "ideal" tissue-specific scaffold should support appropriate biological response via cell-scaffold interaction, whilst providing mechanical and structural support. In MEW, cell-scaffold interaction is strongly influenced by fiber diameter, strand spacing, and overall scaffold layout pattern [42–44]. Notably, a myriad of scaffold architectures is accessible using MEW including but not limited to curved structures, right-angled designs, rectangular shapes with varying strands spacings or even more biologically mimicking scaffolds [7,25,27,45]. Indeed, the presence of a CAD design in conjunction with the utilization of a rotating (mandrel) collector allows to print 3D tube-like structures that have been envisioned for cardiac and renal applications [20,46]. Below, we discuss key aspects that influence MEW scaffolds' design, their role in supporting improved regenerative outcomes, as well as ongoing efforts on translating the fabrication of MEW scaffolds from completely flat to more anatomically relevant surfaces, as only a few DOC tissues are entirely flat.

3.1. Fiber diameter

Commonly, the diameter of MEW fibers tends to be one order of magnitude greater than those obtained by solution-based electrospinning. Nonetheless, the submicron-to-micron scale diameter allows for production of highly-ordered and porous scaffolds [29,35]. Numerous studies have investigated the effect of MEW parameters (*e.g.*, melting temperature, applied electric voltage, pressure, collector speed, spinneret diameter, among others) on the resulting fiber diameter and several groups have systematically explored a myriad of processing parameters in regards to that (**Table 1**). In brief, controlling both polymer dispensing pressure and collector speed permits to create a large spectrum of fiber diameters [35]. Thinner fibers of 3-30 μm are typically formed when the collector speed surpasses the CTS and mechanical stretching of the molten jet [37,39]. In contrast, fiber thickening from 2 μm to 7 μm occurs as a result of high flow rate, *i.e.*, increasing polymer dispensing pressure from 0.5 to 4 bar [35]. In fact, the flow rate of polymer melt appears to be a key factor governing fiber diameter [47]. Nevertheless, these aspects are also valid, without any variations, for the applied voltage, since higher voltages tend to decrease fiber diameter. Thus, adjusting these parameters leads to fibers with well-defined diameters in a scale that more closely mimics the collagen fibers in the native ECM [17]. As elegantly described in a recent review, controlling the electrified jet has prevented the fiber pulsing effect that results in predictability and reproducibility of fiber deposition [18]. Moreover, Hrynevich *et al.* reported the fabrication of a wide spectrum of fiber diameters, ranging from 2 to 50 μm, by alternating both pressure and collector speed [35]. Although further reducing the fiber diameter below sub-micrometer sizes is still challenging, this has been accomplished by the insertion of an acupuncture needle into the spinneret [23]. This adaptation reduced the lumen of the spinneret end edge allowing to reach fiber diameters of approximately 300 nm [23]. This finding might be extrapolated and used while processing nanoscale MEW patterns to DOC applications. Hence, through MEW, in a single-step fabrication process, a multilayer construct intended for a tissue-specific application can leverage MEW nano- to micron-scale fiber capability to reconstruct distinct DOC tissues and tissue interfaces [18,35]. Notably, that is extremely relevant for the regeneration of complex defects involving multiple tissues and tissue-interfaces of hierarchically organized DOC tissues, such as bone, periodontal ligament (PDL) and the temporomandibular joint (TMJ).

3.2. Strand spacing and laydown pattern

Scaffold strand spacing (pore size) and interconnectivity have been considered as two of the most noticeable factors governing cellular response and new tissue formation (**Fig. 3A-D)** [7,42]. In MEW, strand spacing is greatly influenced by the laydown pattern and significantly impacts on the mechanical performance of the scaffolds. In brief, as the spacing area increases from 0.5 mm^2 to 1 mm^2 the axial stiffness drops as high as 48%, indicating that pore area below 0.5 mm^2 provide compacted structures that are more mechanically competent. In contrast, increasing the pore area allows a 20% higher yield strain to make the scaffolds recoverable after deformation [48]. Moreover, from a biological view, MEW scaffolds with strand spacings ranging from 100 μm to 750 μm permits suitable cell attachment, leading to improved cell bridging and proliferation [42,49]. Though larger strand spacing influences cell survival, smaller spacing improves cell viability and neotissue growth [42,49–51]. The effect of strand spacing and shape is also evident in directing cell-cell interaction and phenotype commitment [52]. Therefore, it is possible to guide cell behavior by controlling strand spacing to direct progenitor cells attachment, proliferation, and lineage commitment [27,42].

In the last few years, apart from the conventional box-shaped scaffolds, MEW has proven its ability to make structures with more complex geometries [21,53,54]. For instance, cardiac muscle holds a unique ECM network known to provide structural and mechanical support to cardiac cells. Accordingly, MEW was utilized to develop organized fibers capable of improving cellular response to mechanical anisotropy and guide the alignment of cardiac progenitor cells [21]. Moreover, in a serpentine-shaped layout, the semicircular fibers straighten their shape, allowing for higher extensions under uniaxial tensile load, and approximating the viscoelastic nature of heart valves [45]. The pre-programmed MEW serpentine structures have the potential to recapitulate the wavy architecture and viscoelastic properties of collagen fibers of heart valves, and exhibited mechanical strength similar to conventional materials used in aortic grafts **(Fig. 4A-B)** [45]. Remarkably, sinusoidal MEW patterns displayed non-linear stress-strain behavior and low stress at initial strain under uniaxial tensile loading, thus approximating to the non-linear behavior of crimped collagen fibrils present in tendons and ligaments [55]. Alternatively, the fabrication of other non-linear 3D patterns, *e.g.,* hexagons and auxetics laydown, also enables to achieve elastic deformation [41,56]. These outcomes emphasize the ability of MEW to generate tissue-specific scaffolds/constructs that approximates to the arrangement and biomechanics of the tissue to be regenerated. Thus, the crimped nature and the micro-anatomical organization of collagen bundles within the periodontal ligament (PDL) can be potentially cap-

Table 1
List of studies utilized MEW based technique for fabrication of scaffold and system configurations as well as outcomes. The following abbreviations are used: P (applied pressure), FR (flow rate), V (voltage), CD (collector distance), T (temperature), Vel (collector speed), S (Strand spacing), FD (fiber diameter), M (molecular weight/number), N (needle gauge), and N/A (not applicable).

Polymers & Additives	Parameters	Design	Cell	Outcome Summary	Ref.
PCL	FR=50 µL/h V=12 kV T=70°C CD=3 cm N=21G M=50 kDa	S=20 μm FD=21 µm	N/A	Jet and collector contact located directly below the spinneret must be close to the jet speed for controlled fiber deposition.	[29]
PCL/CaP	FR=50 µL/h V=12 kV T=78°C CD= 4 cm N=21G M=50 kDa	Tubular S=6.9-4.8x10^{-2} mm^2 FD=19.9-27.7 µm	OB	Winding angle (WA) can control scaffold pore (*e.g.*, size, shape, number and porosity). Increasing WA decreases FD and spacing.	[91]
PCL	FR=10 µL/h V=10 kV T=80°C CD= 4 cm Vel=2.5$\times$10^{-2} m/s N=23G M=83 kDa	S=46 µm FD=7.5 µm	Dermal fibroblast	The translational speed of the collector allows for straight fiber morphology in the MEW structure.	[92]
PCL	FR=10-20 µL/h V=4-14 kV T=80-90°C CD=1-3 cm N=21-23G M=80,000 g/mol	Patterned FD=5-35 μm	N/A	Low flow rate, collection distance and high applied voltage allow the production of small FD. In contrast, high flow produces larger FD.	[47]
PCL	FR=40 µL/h V=1.05 kV/mm T=73°C CD=1 cm Vel=750 mm/min N=21G M=N/A	90°-cross-hatched S=1 mm FD=40 μm	MC3T3	Highly ordered 2-mm thick scaffold was produced by use of dual voltage power supply, positive voltage on needle tip and negative voltage on collector plate.	[93]
GelMA/PCL	FR=18, 72 or 180 μl/h V=8–10 kV Vel=1400 mm/min N=23G M=N/A	0° to 90° S=0.2-1 mm FD=19.4, 48.5 and 88.5 µm	Human chondrocyte	Stiffness of the constructs significantly enhanced by enforced PCL/GelMA composite, to achieve values similar to native articular cartilage.	[64]
PCL	P=0.5-4.0 bar V=2-10 kV T=80-120°C CD=1-10 mm Vel=1000-9000 mm/min N=21-33G M=83$\times$10^3 g/mol	0°-90°-Box shape FD= 817 nm S=100.6 μm	N/A	Dynamic balance of MEW processing parameters allows production of high-quality small FD. NCO-sP (EO-*stat*-PO)-coated slide prevents scaffold detachment *in vitro*.	[8]
PCL/ Poly(2-oxazolin)/hydrogel	FR=20 µL/h V=11.7 kV T=120°C CD=1.5 cm N=23G M=N/A	90°-laydown S=200-600 µm FD=23±1 μm	N/A	PAOx copolymers are amphiphilic, therefore PEtOx-ButenOx used to wetting PCL fibers and eliminate defects between PCL and hydrogel.	[32]
poly (LLA-ε-CL-AC)	V=7 kV T=145°C P=3.0 bar CD=4.5 mm Vel= 7 mm/s N=33G M=17900-22600 Da	90°-laydown S=100 µm FD=24.6 µm	N/A	Poly (LLA-ε-CL-AC) photo-cross-linkable amorphous polymer that flows upon heating at intermediate Tm and have high (T_g) rapidly solidify once melt-printed.	[31]
PCL/CaP/ pretreated NaOH	FR=10 µl/h V=11-12 kV CD=2 cm T=100°C N=23G Vel=2000 mm/min M=N/A	0°–90°-laydown S=100 µm FD=18 µm	OB/placenta stem cells	3D endosteal microenvironment of CaP coated scaffold was suitable for growth and migration of HSCs towards bone matrix.	[83]
PCL/star-PEG heparin	FR= 50 µL/h V=10 kV T=78°C CD=4 cm N=21G M=N/A	Tubular scaffolds FD=8.5 µm	HUVEC and BM-MSC	*in vivo* multiphasic platform has been constructed to simulate both the cellular and morphological components of periosteum	[88]

(*continued on next page*)

Table 1 (*continued*)

Polymers & Additives	Parameters	Design	Cell	Outcome Summary	Ref.
PCL/sPEG/Hep hydrogels	FR=20 µL/h V=12-12.5kV Vel=0.7m/min T=100°C CD=15 mm N=23G M=N/A	0°–90°-laydown S=200-600 µm FD=21.36 µm	Human chondrocytes	The combination of star poly (ethylene glycol) / sPEG / Hep/PCL produces mechanical anisotropy, similar to cartilage microenvironments.	[65]
Polypropylene (PP)	P=0.5-1 bar V=6.2 kV T= 215°C CD=3.3 mm N=25G Vel=0.625-750 mm/min M=N/A	90°-laydown S=0.2-1 mm FD=16.4 µm	N/A	PP provides different designs of fibrous textiles for use in medical applications.	[30]
pHMGCL/PCL	pHMGCL: P=2 bar V=5 kV CD=3 mm Vel=5 mm/s M=39 kDa PCL: P=3 bar V=7 kV CD=3 mm Vel=25 mm/s T=87-94°C M=71 kDa	Rectangle/square S=150 µm FD=3-12 µm	Cardiac progenitor cells	MEW of pHMGCL/PCL, triangular pattern approximates the mechanical properties of native myocardial component and promote CPC's alignment for cardiac engineered tissues.	[21]
PCL/GelMA	P=2 bar V=7 kV T=75°C, 70°C Vel=0.3 m/min N=23G M=95–140 kDa	Laydowns 0-90°, 0-60° or 120° S=250 or 750 µm	hBMPCs	Tuned biomechanical properties of *J*–shaped σ–ε curve (up to a strain of ~0.40) distinct phases (toe, heel and linear) resemble collagen fibril.	[10]
poly (methyl methacrylate)	V=3 kV T=250°C CD=500 µm-5 mm Vel=15 mm/s M=N/A	FD=500 nm to 6 μm	N/A	Method for fabrication of a micro/nano-optical fibers MNOF based on near-field melt electrospinning.	[94]
PCL	P=0.8,1.5 or 2.6 bar V=8, 11 or 12 kV T=65°C CD=12 mm Vel=1700,1200 or 700 mm/min N=23G M=95-140 kg/mol	0-90° or 0-60° laydown FD=3-30 µm	N/A	Small fibers of ~ 3-10 µm, is accessible when coordination is achieved between low pressure, moderate voltages and high collection speed. In contrast, high pressure allows for polymer flow and larger FD ~ 10-20 µm.	[39]
PCL	P=1.9 bar V=5.6 kV CD=4.5 mm T=96°C N=25G Vel=3500 mm/min M=N/A	Box-shape S=100-350 µm FD=7 µm	HUVECs and NHDF	Orientation of capillary-like structures, and guidance of neovascular-like structures to the center of the pores, dependent on the pore size of the scaffolds.	[86]
PCL/pHEMA	P=2.0 bar V=6 kV T=90°C Vel=900-1200 mm/min CD=3mm N=25G M=N/A	FD=13.3 µm	N/A	Out-of-plane deposition of an electrically charged polymer melt, resulting in stabilizing fibers, increased the shear modulus could potentially be used to reinforce hydrogels.	[67]
PCL/GelMA	P=3.0 bar V=5.5 kV Vel=10 mm/s T=90°C N=23G M=N/A	S=200, 400, 600 or 800 µm FD=20 µm	N/A	MEW/hydrogel reinforcement includes fibers being pulled in tension to create lateral expansion of the hydrogel and the interconnections create multiple interlocking.	[66]
PCL	V=7, 8, or 9 kV CD=8-18 mm M=N/A	S=1000 µm FD=20 µm	PDL cells	Computational modeling provides numerical values of variable working distances to maintain the electrostatic force at constant level for ~7 mm height MEW construct.	[40]
DMS-A12-HMDI	P=1-3 bar V=8-12 kV T=80-100°C CD=8.5 mm M=N/A	FD=10 to 20 µm	N/A	FD is significantly influenced by the applied voltage and fiber fusion effects at the intersections allow to build a MEW construct in height.	[33]

(*continued on next page*)

Table 1 (*continued*)

Polymers & Additives	Parameters	Design	Cell	Outcome Summary	Ref.
PCL	P=0.5-4 bar V=7 kV T=73°C CD=6 mm N=22G M= N/A	S=300 µm FD=2-50 µm	hMSCs	When the speed of the collector is kept above the CTR, the highest accuracy of MEW can be achieved. The FD can be adjusted by FR and collector speed.	[35]
PCL	P=10 to 50 kPa V=8, 10, 12 kV T=80, 90 or 100°C CD=20 mm N=21G M= 80,000	90°, 45°, 10° or round S=300 µm FD=10.4 µm	hSSCs	Fiber orientations dictate cell morphology, mechanosignalling and lineage commitment. Cells cultured in 90° laydown have shown a lower aspect ratio, greater spreading, greater cytoskeletal tension and nuclear YAP expression.	[82]
PCL/GelMA	P=1 Bar V=5 kV T=85°C CD=6 mm Vel=80 mm/s M=N/A	Square S=100, 200 or 400 µm FD=13 µm	Equine-derived (eMSCs)	MEW/hydrogel provides mechanically and biologically competent constructs, enhances MSCs differentiation into cartilage.	[77]
PCL	P=0.8-2.2 bar V=8-12 kV T=70-95°C Vel=1-3x10^3 mm/min M=N/A	Small	N/A	The degree of the electrostatic acceleration is correlated to the charge density of polymer melt and flow properties.	[37]
PCL/MATRIGEL	P=3 bar T=80°C M=N/A	Square S=100, 200 or 400 µm FD=9.7mm	Ltk-11 fibroblast	Electrophysiology of a glycine receptor-transfected Ltk-11 mouse fibroblast in MEW/reinforced Matrigel	[54]
PCL	FR=400 mm/min P=1.2 bar V= 6 kV T=73°C M=N/A	0°-90° box shape S=225, 300, 375, 450 or 500 μm FD=20 μm	MG63	Box-shaped construct with pore sizes between 225 μm and 500 μm, allows for osteoblast attachment and differentiation.	[50]
PCL/CaP	P=1.16 bar V=11 kV T=90°C M=N/A	S= 100 µm FD=10 or 13 μm	OB and PBMC	Cell/non-mineralized ECM density in scaffold cultured OB or OB+PBMC, *in vitro* system for bone regeneration.	[95]
PCL	P=1.2 bar V=11 kV T=73°C CD=4 mm Vel=400 mm/min N=22G M=N/A	90°/0° or 60° S=200 µm FD=20 μm	MG63, HaCaT and L929	Different geometries of MEW scaffolds were individualized for OB attachment on one side and for keratinocytes on the other side. Film casting formed core for bacteria-tightness.	[51]
PCL	P=0.5-1.2 bar Vel=500-1500 mm/min M=N/A	Box-shape S=360 µm FD=13-15 µm Catching S=130 µm FD=7-8 µm	ASC-Spheroid	MEW construct tailorable to spheroid size were seeded with ASC spheroids, to further utilization for adipose tissue regeneration.	[44]
PCL/CaP cement	V= 12 kV CD=2mm 27G Mw= N/A	Box-shape S=200, 500 or 1000 µm FD= 8 µm	N/A	Treating PCL with NaOH increases strength and maintains high fracture energy ~1.5 to 2.0 mJ/mm^2 for application in planar or curved cranial defects.	[96]
NCO-poly(ethylene oxide-stat-propylene oxide) /PCL	P=1.9 bar V=5.6 kV T=96°C CD=4.5 mm N=25G M=N/A	0-90-Box-shaped S=200 µm FD=7 µm	Primary hMSCs	Photo-leucine is covalently immobilized into the sP(EO-stat-PO) results in a photoactivatable scaffold that enables binding of sterically demanding molecules.	[97]
PCL/SrBG	P=0.050 MPa FR=2.39 mm/min V=6 kV T=55°C CD=10 mm M=37,000 Da	Square-crosshatch S=1 mm	N/A	Platform of high ceramic-content polymer scaffolds for applications in bone tissue engineering was successfully processed.	[98]
PCL	FR=25 µl/h V=10-12 kV Tm=78°C N=21G Vel=80 mm/s M=45,600 g/mol	0–90° or 0–45° S=19 or 35 µm FD=5 or 7 μm	Fibroblast (NHDFs)	Bioinformatics-guidance of single-cell confinement are modeled. Unlike flat surface, cells develop cluster of mature FAs at 0–45°.	[99]

(*continued on next page*)

Table 1 (*continued*)

Polymers & Additives	Parameters	Design	Cell	Outcome Summary	Ref.
PCL	P=2 bar V=6-6.5 kV T=85°C CD=4.5 mm Vel=280 mm/min N=23G M=N/A	Serpentine FD=0.5 or 1 mm S=0.25, 0.5, or 1 mm	vascular smooth muscle	The serpentine structure reproduces the J-shaped strain hardening behavior and anisotropic composition of natural valve leaflets.	[45]
Milk proteins/PCL	P=100 kPa FR= 12 mm/s V=20 kV T=85°C M=50 kDa	90°-angle S=300 μm FD=50 µm	Keratinocyte & Fibroblast	Increased cell growth and infiltration into PCL/MP scaffolds have potential in dermal tissue regeneration.	[100]
PCL	P=70 kPa T=80°C CD=1.5 mm Vel=3 mm/s M=43 kDa	Square/rectangle S=200 µm FD=0–50 µm	N/A	Decreased FD when stage speed is decreased and T increased, and vice-versa. Tailoring the parameters provides structural anisotropy mimic native ECM	[53]
PCL/CaP	P=2.2 bar V=10.1 kV T=74-85°C N=23G M=95–140 kDa	0°–90°' S=150 µm FD=12 µm	hPOB & prostate cancer	MEW simulate the bone-like 3D microenvironments and produce *in vitro* model to study metastases in bone.	[26]
PCL	P=10 kPa V=10 kV T=90°C N=21G CD=2 cm Vel=17 mm/s M= 80 000 g/mol	Square S=100, 200, or 300 μm FD=4.01 µm	hMSC	Small pore size of 100 µm is optimal for hMSCs as it demonstrates the highest global stiffness, local fiber stiffness and enhances mineralization.	[52]
PCL	P=10 kPa V=7 kV Tm=77°C CD=1.4 mm Vel=950 mm/min N=30G M=N/A	Box, triangle, round or disordered S=40=100 µm FD=2.6-2.9 µm	Monocyte	Geometry and spacing from 100 to 40 μm facilitate macrophage elongation and polarization, an evidence to consider the design of biomaterials to positively impact tissue regeneration.	[43]
PCL/CaP	FR=20 mL/h V=5-7 kV T=80°C CD=10 mm N=21G M=N/A	30 and 50% layout FD=6-10 μm	hOB	Offset and gradient scaffold have shown to upregulate ALP activity and matrix mineralization of osteoblasts.	[42]
α-TCP/hydrogel/PCL	P=1.5 bar T=90°C Vel=50 mm/s V=10 kV M=N/A	Box-patterns S=300 μm FD=10 μm	ACPCs and MSCs	Hydrogel/ceramic enhances adhesion strength >6.5-fold, enables structural stability in *ex vivo* osteochondral defect.	[74]
PCL	P=0.05 MPa V= 4.5 kV for flat and 5.5 kV for tubular T=86°C N=21G Vel=900 mm/min M=37,000 Da	90°, 50° or 20° crosshatch/gradient/ and tubular S=850-250 μm FD=3-16 mm	MC3T3	Customized pattern generation software was developed to enable the design of MEW scaffolds.	[48]
PCL/Purasorb PC 12	P=180 kPa V=8 KV T=75°C CD=10 mm N=23G Vel=1000 mm/min M=N/A	S=200 µm FD= 10-20 μm	hMSCs	Bone-Ligament-Bone (BLB) / cell sheets constructs enhanced mechanical properties regardless of the pattern and fiber orientation and induced spontaneous cell organization.	[81]
PCL/Matrigel	P=3 bar V=6 kV T=80°C CD=4 mm N=25G M=N/A	Crosshatch S=200 µm	Cortical neuronal cells	Reinforced Matrigel enhanced cortical neurons viability, maturity, and faster dendrites formation as a potential 3D study model of neuronal networks.	[89]

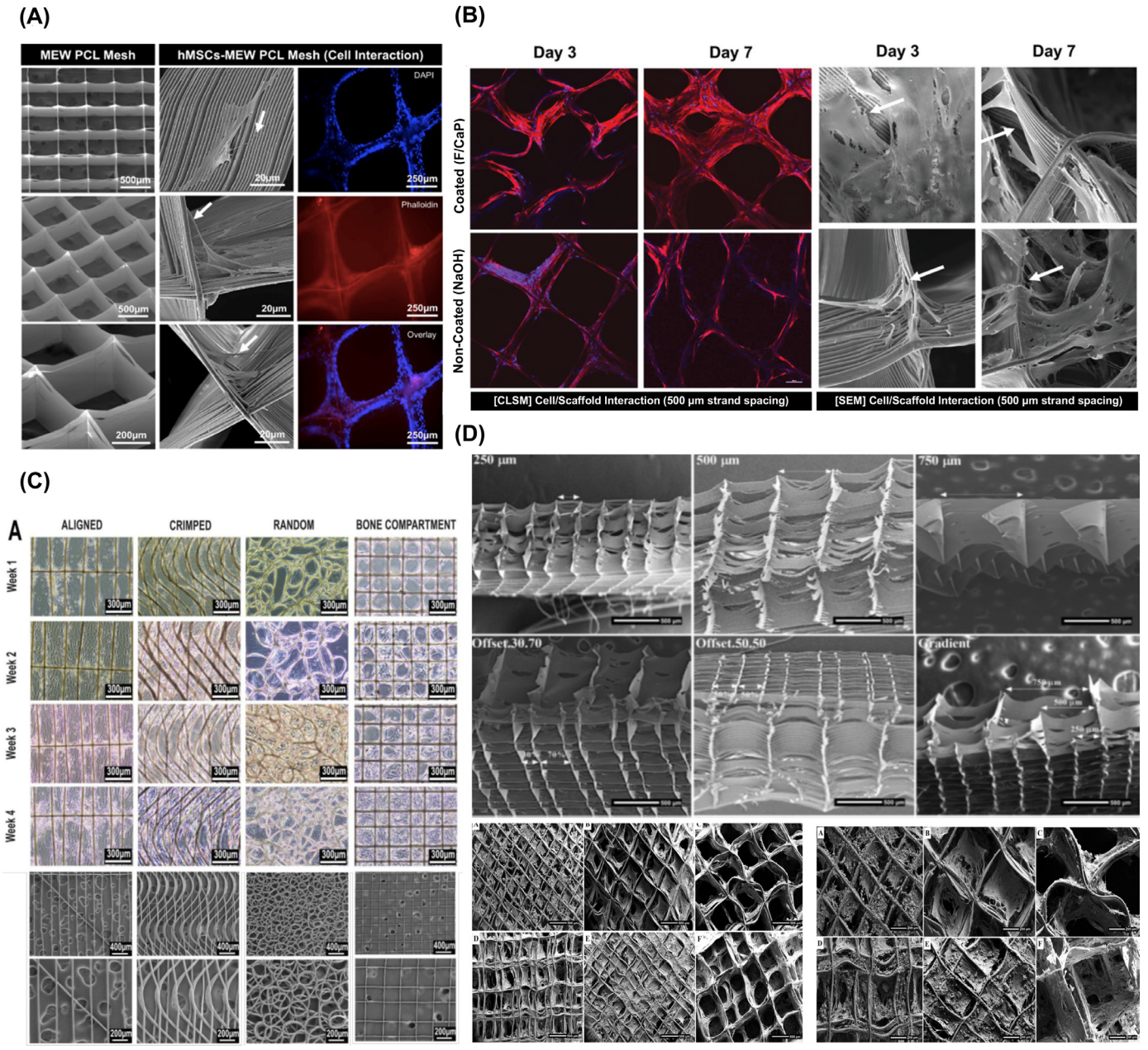

Fig. 3. Cell's behaviors in various MEW design. **(A)** Well-aligned (0-90°-oriented junctions) fibrous 3D architecture with 500 µm strand spacing shows human-derived mesenchymal stem cells (hMSCs)/MEW poly(e-caprolactone) scaffold interaction. From Dubey *et al.* (2020) [7]. **(B)** Confocal microscopy images and SEM images show significant hPDLSCs bridging in 500 µm F/CaP-coated scaffolds and non-coated scaffolds after 7 days. Note pronounced cell spreading was detected along the nanostructured F/CaP-coated scaffolds (white arrows indicate important filopodia protrusion along and around the fibers). From Daghrery *et al.* (2021) [27]. **(C)** MEW fiber orientation and cellular organization in anterior cruciate ligament tissue engineering. From Gwiazda *et al.* (2020) [81]. **(D)** SEM images of highly-order MEW porous and gradient scaffolds and mineralization of hOB on MEW scaffolds after 30 days of culture. From Abbasi *et al.* (2020) [42].

tured through similar MEW designs. Ultimately, these concepts can also be extrapolated to mimic native temporomandibular ligament functions on controlling physiological mandibular movements and the stability of the disc. However, due to multi-tissue architectures, a graded scaffold resembling the biological and physiological properties of the TMJ and bony interface, is a major foreseen limitation.

3.3. Voluminous constructs

For the fabrication of voluminous constructs, typically above 2-mm thick, accurate fiber stacking has been considered a significant technical hurdle. This has been attributed to remnant electrical charges trapped in already deposited fibers, and the "jet lag" phenomenon, where the electrified molten jet is deposited on the collector at a discrete distance behind the position of the spinneret [29]. That slight difference is more evident as the number of layers increase, which in turn affects the accuracy of the construct [29]. Indeed, the fabrication of scaffolds mimics not only the structural complexity of a given tissue but also resembles its size, which is one of the end goals for tissue regeneration. Strikingly, Saidy *et al.* have successfully replicated the complex geometries of real-size aortic root and sinus of Valsalva using a two-component collector to minimize electric field instabilities and improve control on the fibers' deposition **(Fig. 4C)** [57]. It is also noteworthy that MEW has been employed to obtain degradable medical devices for cardiac purposes. For instance, coronary stents composed of PCL and

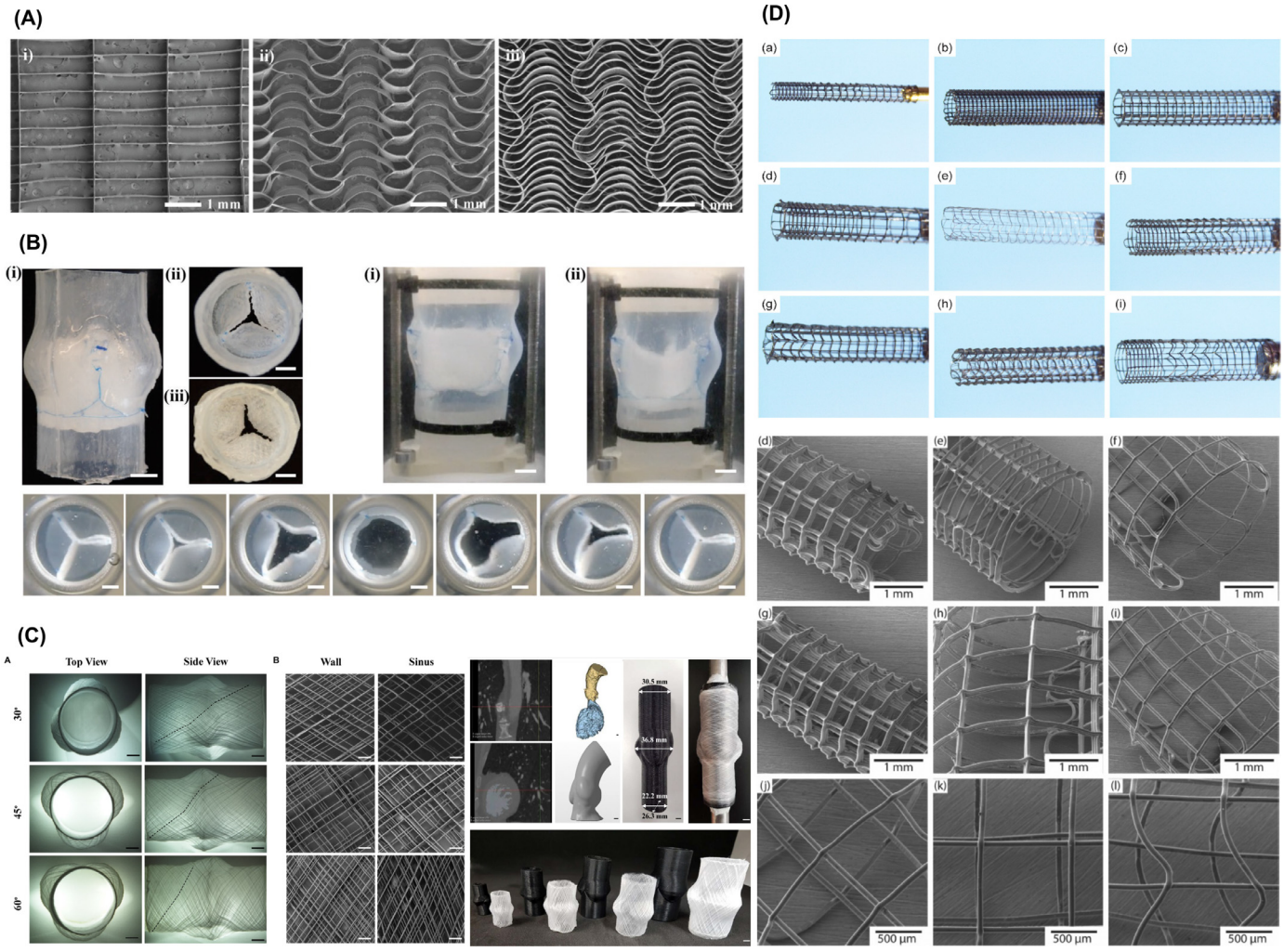

Fig. 4. Biomimetic print designs of MES scaffolds. **(A)** Biomimetic serpentine patterns design for heart valve tissue engineering and **(B)** Custom-made flow loop system, where the MEW scaffold is sutured into a silicone aortic root as single leaflets and functionality assessment of the opening and closing sequence of the valve. From Saidy *et al.* (2019) [45]. **(C)** Characterization of scaffolds printed at 30°, 45°, and 60° winding angle for fabrication of personalized aortic root scaffolds. From Saidy *et al.* (2020) [57]. **(D)** Macroscale and microscopic images of MEW-based personalized biodegradable coronary stents. From Somszor et al., 2020 [46]..

reduced graphene oxide were combined to prepare stents in various diameters and architectures. The constructs demonstrated the ability of being crimped and re-expanded to enable catheter action, and interestingly improved endothelialization of seeded human umbilical vein endothelial cells (HUVECs) (Fig. 4D) [46]. Complementary, a machine vision system reported by Mieszczanek et al. [58] provides real-time monitoring and visual information to precisely define the processed fiber diameter in correlation to electrified jet properties – thus enabling the fabrication of collapsible tubular structures by attaining constant electric field . These findings contribute to designing patient-specific scaffolds and moving towards translating the technology to the clinical realm [46,58]. Meanwhile, the physical principles correspondent to limited volume of MEW constructs have been studied [40]. Variable working distances were established via a computational modeling system to maintain constant electrostatic forces during printing. The established computational simulation allows for the production of highly-ordered large volume constructs of maximum height ca. 7 mm by alternating voltage profiles. Nonetheless, the control over the microscale layer shifting has permitted the creation of tilted walls in a construct. Outstandingly, modifications in the amplitude (*i.e.*, a layer-on-layer shift in the range of the printing paths), inward, and outward tilts, were controlled to foster the overhanging design (**Fig. 5A**) [24]. This strategy opens new prospects on designing nature-inspired scaffolds for applications in regenerative dentistry, where a supportive interfacial layer is needed between structurally and mechanically dissimilar soft and hard tissues, such as cementum-PDL or PDL-bone. Moreover, it brings new opportunities to replicate the circular shape of osteons observed in native mature cortical bone.

It is important to mention that up until now, a few regenerative principles have been applied to dentistry, considering the complex anatomy of tooth structures, mineralized enamel, dentin and soft-core dental pulp, as well as the surrounded periodontium (*i.e.*, alveolar bone, PDL, cementum, and gingiva). To build such structure a high-resolution volumetric complex that could support the tissue properties diversity in each layer is needed. Conceptually, Liashenko *et al.* have created layer-by-layer deposition of polymer melt with a higher level of accuracy not only to produce 3D constructs but to fabricate ultrafast high resolution self-assembly constructs exploring the advantage of electrohydrodynamic (EHD) jet deflection printing (**Fig. 5B**) [59]. This strategy has the potential to unlock some of the current limitations of MEW, *i.e.*, fabrication of large volumes and decrease fabrication time. These contributions

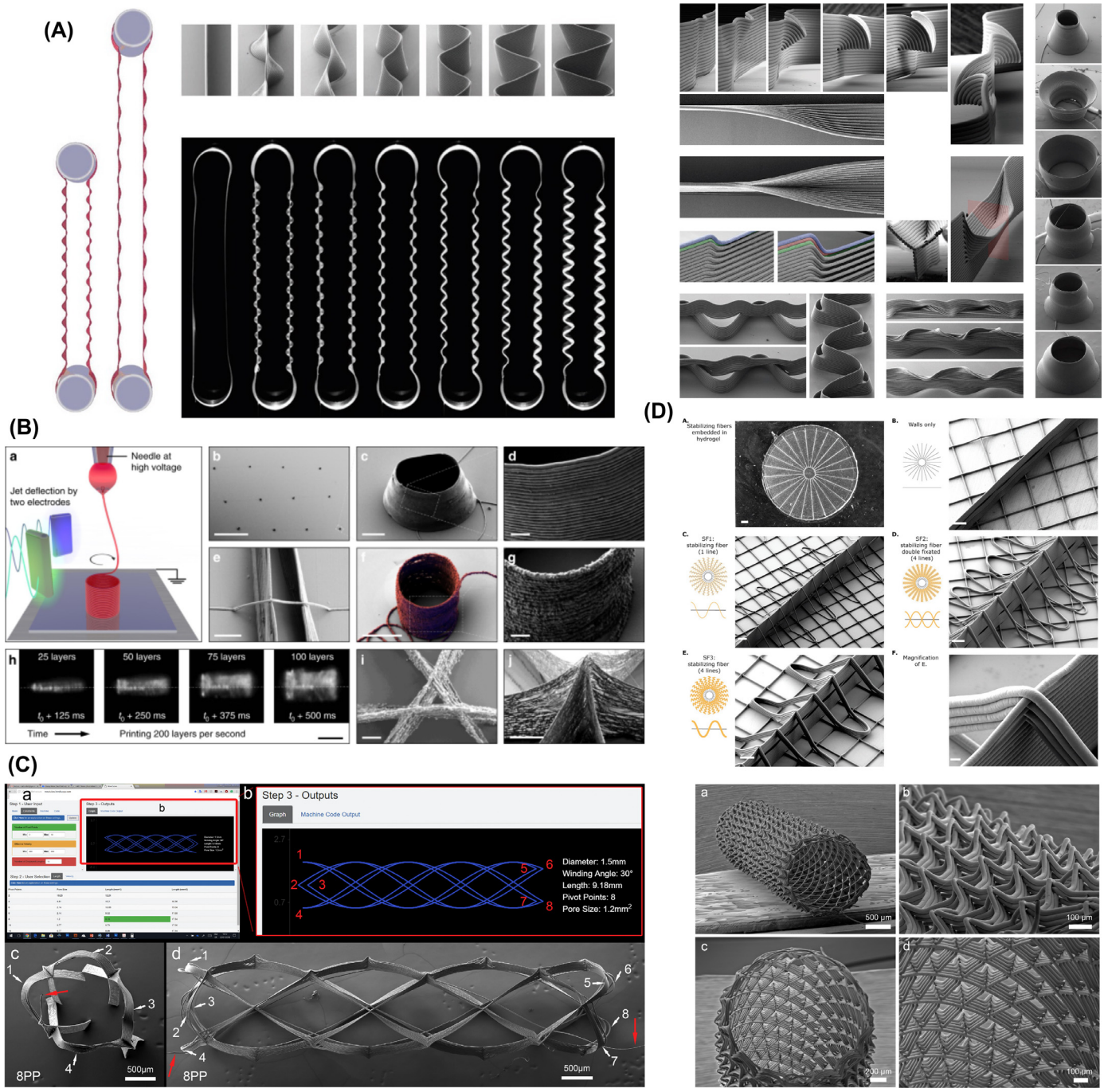

Fig. 5. Various complex MEW scaffold design. **(A)** Novel complex overhanging structures by controlled layer shifting and multiphasic walls formed by an abrupt change in printing trajectory. From Liashenko *et al.* (2020) [24]. **(B)** Ultrafast 3D printing of cylindrical microstructures single suspended polyethylene oxide (PEO) fiber bridging a gap between 2 parallel nano wall using electrostatic jet deflection. From Liashenko *et al.* (2020) [59]. **(C)** Web-based application, showing the printing path for an eight pivot point, to generate printing path for porous tubes like structure for TE. From McColl *et al.* (2018) [19]. **(D)** Variants of stabilizing fibers produced in a radial manner. From Ruijter *et al.* (2018) [67].

would be pivotal to direct the path of building tissue-specific constructs to regenerate a variety of DOC tissues affected by trauma, disease, or congenital anomalies.

3.4. From flat to anatomically relevant architectures

To date, the majority of MEW research has focused on an "in-plane" printing approach, where structures are manufactured in the same plane as the substrate/build plate. In almost all instances this signifies that structures are laid down onto a flat substrate. In addition, to ensure a constant electrostatic force, which is responsible for pulling the fibers in MEW, the substrate/build plate is typically composed of conductive metallic materials, such as copper, stainless steel, or aluminum. Obviously, these inherent requirements do not represent the resorbable biomaterials and natural anatomical structures that regenerative dental medicine aims to recreate [25]. Recent reports have shown that MEW can also accurately print microstructured fiber meshes into anatomically relevant shapes (**Fig. 4 and Fig. 5**), such as convex-shaped structures, and onto clinically relevant biomaterials, including hydrogel, bio-

ceramics and thermoplastics [25,60]. These findings have been applied to the fabrication of anatomically-shaped MEW scaffolds that can follow the contour of a diarthrodial joint surface, which could also be uniquely applied to osteochondral interfaces of the temporomandibular joint (TMJ).

In a few other recent studies, researchers have included a 4th rotary axis beneath the deposition printhead to develop more complex geometries on cylindrical mandrels. McColl *et al.*, developed an advanced tool of web-based mathematical application for planning continuous direct-writing path complex tubular frame of diameter as small as 1.5 mm **(Fig. 5C)** [19]. Equally innovative, MEW was effectively deployed to create tubular scaffolds replicating kidney tubules [20]. Rhombus-shaped constructs mimicking kidney's proximal tubules were engineered to facilitate exchanges with vasculature and improve the filtration process [20]. The ability to develop tubular structures has tremendous clinical value not only for engineering vascular structures but also for salivary glands regeneration after tumor resection and/or irradiation. Apart from that, DOC structures such as the TMJ and periodontal tissues are under continuous loading which is critical for material design. A material with negative Poisson's ratio, for example auxetic materials that expand rather than contract upon loading may support blood vessels against collapse and allow regeneration [61]. Recently, Paxton *et al.* obtained auxetic tubular scaffolds via MEW. Upon loading, the material showed 80.8% increase in diameter and Poisson's ratio of − 5.8 [61]. Collectively, these extraordinary findings emphasize that the design freedom of MEW has translation potential in the development of patient/defect-specific scaffolds for complex functional tissues and thus hold great impact in DOC tissue regeneration. Given the fact that DOC tissues are hierarchically organized structures, composed by multiple cell types and ECM components, a single fabrication process and/or processing material cannot precisely establish the regenerative process.

4. Convergence of materials and technologies to fabricate hierarchically complex architectures

In order to engineer complex living architectures that could approximate to the structure and composition of DOC tissues, the combination of materials and MEW with other printing technologies is fundamental. Hence, hierarchically defined structures composed of interconnected pores that offers significant increase in overall mechanical properties, provides both haptotaptic and mechanotransducive environment for cells to establish the regenerative process.

Hydrogels are a major biomaterial class in tissue engineering. It contain significant amounts of water (≥ 10% of their volume) [62], and classically, provide an optimal 3D microenvironment for cells comparable to the non-fibrillary part of the ECM of native tissues [63]. Although hydrogels have been used to support cellular differentiation, they are intrinsically soft and lack the mechanical competence needed for load-bearing applications [32,64]. Therefore, hydrogel reinforcement using well-organized, low volume fraction polymeric meshes obtained by MEW offers an opportunity to imitate both the biological and mechanical microenvironments of native human tissues, such as articular cartilage, periodontium, and TMJ [64]. The customizable network composites of hybrid hydrogels and MEW meshes, emulating a fluid-saturated environment and organic stretchable curvy structures, were successfully obtained to resemble collagen fiber architectures of cartilaginous tissues **(Fig. 6A)** [65]. Worth noting, the mechanism of reinforcement with the soft hydrogel combined with MEW fibers, when loaded in compression, is based on the tensioning of the thin polymeric fibers upon lateral displacement of the regenerative hydrogel component. Additionally, multiscale and Finite Element modeling revealed that the fiber interconnections further contribute to this significant load carrying-ability of the hybrid structures [66]. The large magnitude of reinforcement (>50×) at low fiber fraction is especially exciting as the design possibilities of the organized support structures are extensive and still remain to be fully explored, particularly for the reconstruction of DOC tissues.

Remarkably, the capacity of MEW/Hydrogel-based constructs as biomimetic approaches can be further maximized via incorporation of therapeutic drugs and/or bioactive molecules for dentin-pulp complex and periodontal tissue regeneration. For example, we recently reported on the use of MEW PCL fibrous meshes to tune the mechanical properties of amorphous magnesium phosphate (AMP)-laden gelatin methacryloyl hydrogel for bone regeneration **(Fig. 6B)** [7]. Besides, the mechanical reinforcement, the presence of AMP favored *in vivo* bone formation [7]. Worth mentioning, additional design modifications such as the combination of "out-of-plane" MEW constructs, purposely geared to stabilize an existing structure, has shown to amplify the shear modulus of composites, regardless of gel percentage and crosslinking density **(Fig. 5D)** [67]. Taken together, although the use of polymeric MEW meshes to strengthen hydrogels showed promising results when exposed to compressive or shear loading conditions, the complex combination of compressive, shear, and tensile stresses that most human tissues are subjected to, particularly in tissues such as those in the DOC complex, has not been fully elucidated.

Despite the encouraging outcomes of fiber-reinforced hydrogels, the integration of MEW reinforcing structures into a hydrogel typically requires a two-step fabrication process, where the reinforcing construct is first fabricated and only then embedded within a cell-free or cell-laden hydrogel. The aforementioned approach limits the freedom of design of the fibrous architectures, as well as the use of multiple materials and cell types observed in the DOC region. Similarly, even though biphasic scaffolds using FDM and MEW [68], MEW and CaP-coated FDM constructs **(Fig. 7A)** [69,70], or the combination between electrospinning and MEW [71] for hard and soft tissue compartments in bone and ligaments have demonstrated improved interconnectivity and regenerative capacity, their multiphasic architectures are mostly achieved by merging techniques and materials in post-fabrication steps (*e.g.*, structures/compartments bonding). In this way, the wise integration of MEW with other bioprinting methods (*e.g.*, extrusion-based bioprinting) into a single biofabrication platform is desirable [11,72]. Although MEW convergence with other bioprinting technologies is reasonably new, first reported in 2018, multiphasic scaffolds can be obtained in a single-step by alternating parameters such as lay-down patterns, collector speed, and extrusion pressure, thus facilitating multi-tissue and tissue-specific scaffold fabrication [35,73]. In a recent study by our group, bilayered microfibrous MEW scaffolds, that combine a superficial tangential zone (STZ) formed by a densely distributed crossed fibrous mat and a middle and deep zone (MDZ) built as a uniform box-like architecture were able to capture the characteristics of native cartilage STZ and MDZ zones [73]. Importantly, the incorporation of a viable STZ reinforcing layer improved the load-bearing capacity of the engineered constructs, mostly when incongruent surfaces are subjected to compressive stresses. Meanwhile, a clinically promising strategy ingeniously converged MEW and bioceramic printing to engineer hard-to-soft tissue interfaces **(Fig. 7B)** [74]. Likewise, the fabrication of polymeric scaffolds via MEW with a heterogenous gradient of strands spacing led to improved bone formation *in vivo* **(Fig. 7C)** [75].

To validate the design approaches in a non-empirical way, a numerical-based method has been developed for patient-specific soft network composites [76]. The *in silico* design library facilitates materials selection with appropriate architecture to adopt the zonal variation in tissue interface comparable to native tis-

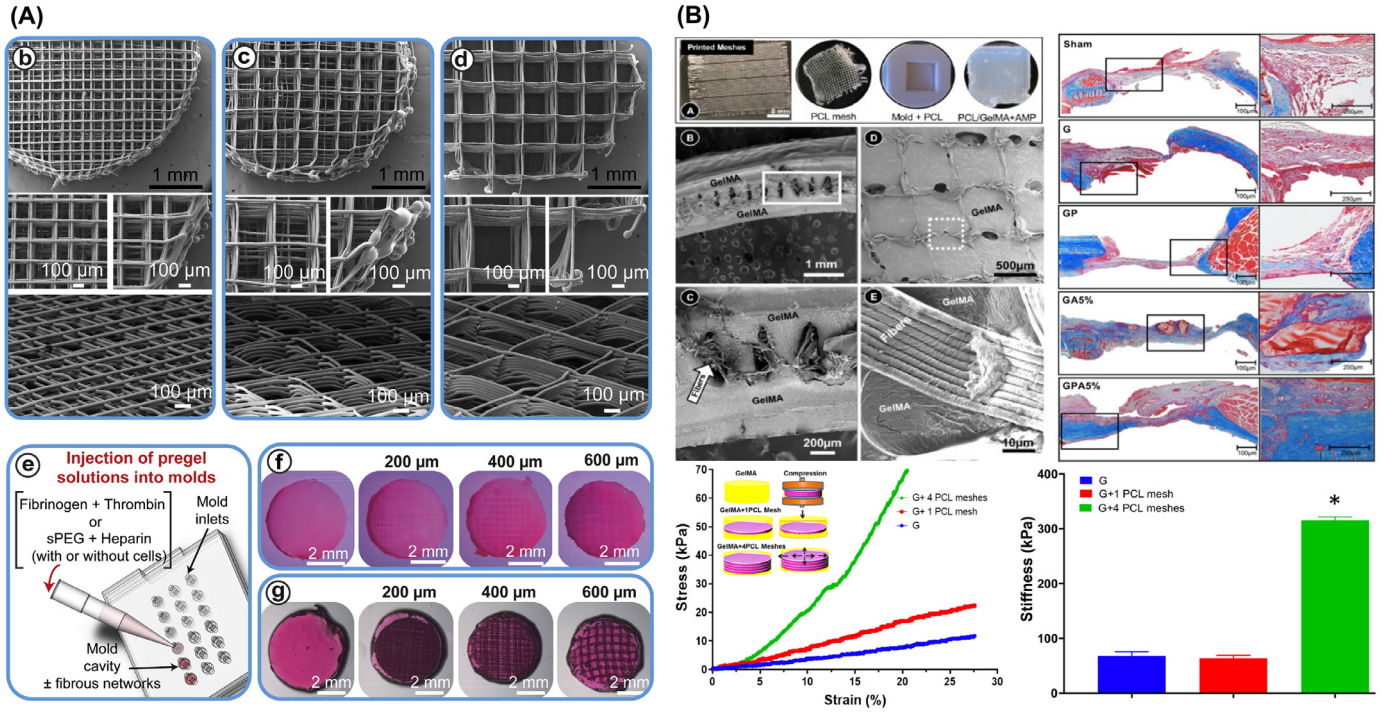

Fig. 6. MEW–hydrogel reinforced composite approaches. **(A)** MEW enabled a good control intended 0°-90° crosshatch at 200 μm, 400 μm, and 600 μm fiber spacing for fiber-reinforced hydrogels of fibrin, sPEG/Hep and hydrogels. From Bas *et al.* (2017) [65]. **(B)** Amorphous magnesium phosphate (AMP) modified gelatin methacryloyl (GelMA) hydrogel infiltrated highly porous MEW PCL meshes with well-controlled 3D architecture. Note the hydrogel phase uniformly infiltrated within the highly order porous structure. Stress-strain curves and stiffness of GelMA indicates higher results when increasing the number of PCL meshes. From Dubey *et al.* (2020) [7].

sues [76]. The systematic evaluation of design parameters and their relation to the mechanical properties provides critical insights to fabricate multiphasic constructs. This is particularly important for predictably managing the coordinated and simultaneous neoformation of hard and soft tissues, and their interfaces (*e.g.,* bone-PDL). Noteworthy, DOC tissues comprise architecturally complex shapes, hence engineering those structures requires tissue-specific approaches, provide cellular instructive cues at spatial and temporal levels. In this sense, a single platform of convergence 3D (bio)printing technologies yield resolution and spatial control for optimal cell distribution and improved biomechanics. A higher level of reinforced forms of hydrogel/MEW constructs by alternated printing of both hydrogel and MEW has been established [77]. In a forward-looking study, Ruijter *et al.* described the convergence between bioprinting and MEW in a single biofabrication approach, which allowed the assembly of mechanically-competent constructs with spatial distribution of distinct types of cells without jeopardizing mesenchymal stromal cells viability and differentiation capacity **(Fig. 8A)** [77]. In sum, the convergence of complementary biofabrication tools (*e.g.*, 3D (bio)printing and MEW) has the potential to yield scaffold systems that would control the dynamics of cell commitment in compartmentalized tissues and interfaces transition. This would possibly represent creating constructs able to recognize and adapt to the continuous changes of the microenvironment and support tissue growth. Conspicuously, Constante *et al.*, reported novel shape morphing anisotropic patterns using 4D printing, based on programmed deposition of MEW fibers and extrusion printing of methacrylated alginate hydrogel that supported the alignment of myofibroblasts to a high degree **(Fig. 8B)** [78].

5. Extending MEW for bioprinting with cell-laden hydrogels

Ink-based bioprinting platforms support the processing of soft yet robust hierarchical 3D structures comparable to those traditionally produced using a hydrophobic polymer such as PCL. The concept of self-crosslinked polymer based on poly(2-ethyl-2-oxazine) has been translated to fabricate chemically crosslinked structures at ambient conditions via MEW [79]. Moreover, supramolecular hydrogel network of ureido-pyrimidinone (UPy) coupled to poly(ethylene glycol) (PEG) chain, shows overall enhancement of mechanical and processing properties. UPy-PEG scaffold presented anisotropic post-swelling behavior and maintain the morphological mesoscale fiber structure [79].

Notably, electrical conductivity of the hydrogel remains a critical challenge for ElectroWriting printing of hydrogels. Strikingly, formation of stable jet is a key prerequisite for MEW. In this regard, Castilho et al. reported considerably higher values of electrical conductivity of the gelnor and silk fibroin hydrogels, with and without poly(ethylene oxide), (0.9–1.3 mS/c) compared to semiconductive fluids (<10–11 mS/cm). Despite that these high conductivity values did not prevent stable jet formation and continuous fiber collection, although limited to 30 min mostly due to hydrogel drying [28]. In detail, Castilho *et al.*, described the concept of cell electrowriting (CEW) to print highly-ordered cell-laden hydrogel-based bioinks through a modified MEW device at ambient conditions **(Fig. 8C)** [28]. By engineering two photo-responsive hydrogel bioinks based on protein-based polymers with different gelation chemistry (gelatin and silk fibroin) – compatible with electrodeposition principles, the authors [28] demonstrated the fabrication of 3D ordered cell-laden constructs (squares, hexagons, and curved patterns) with reduced fiber diameters (5 to 40 µm) that supported and maintained high cell viability post-printing. In sum, the integration of fiber technologies with extrusion- or electrohydrodynamic-based bioprinting enhances control over spatial and local disposition of distinct cell types and superior mechanical competence of bioprinted constructs, while simultaneously expanding manufacturing capabilities to better reproduce local composition of cellular microenvironments.

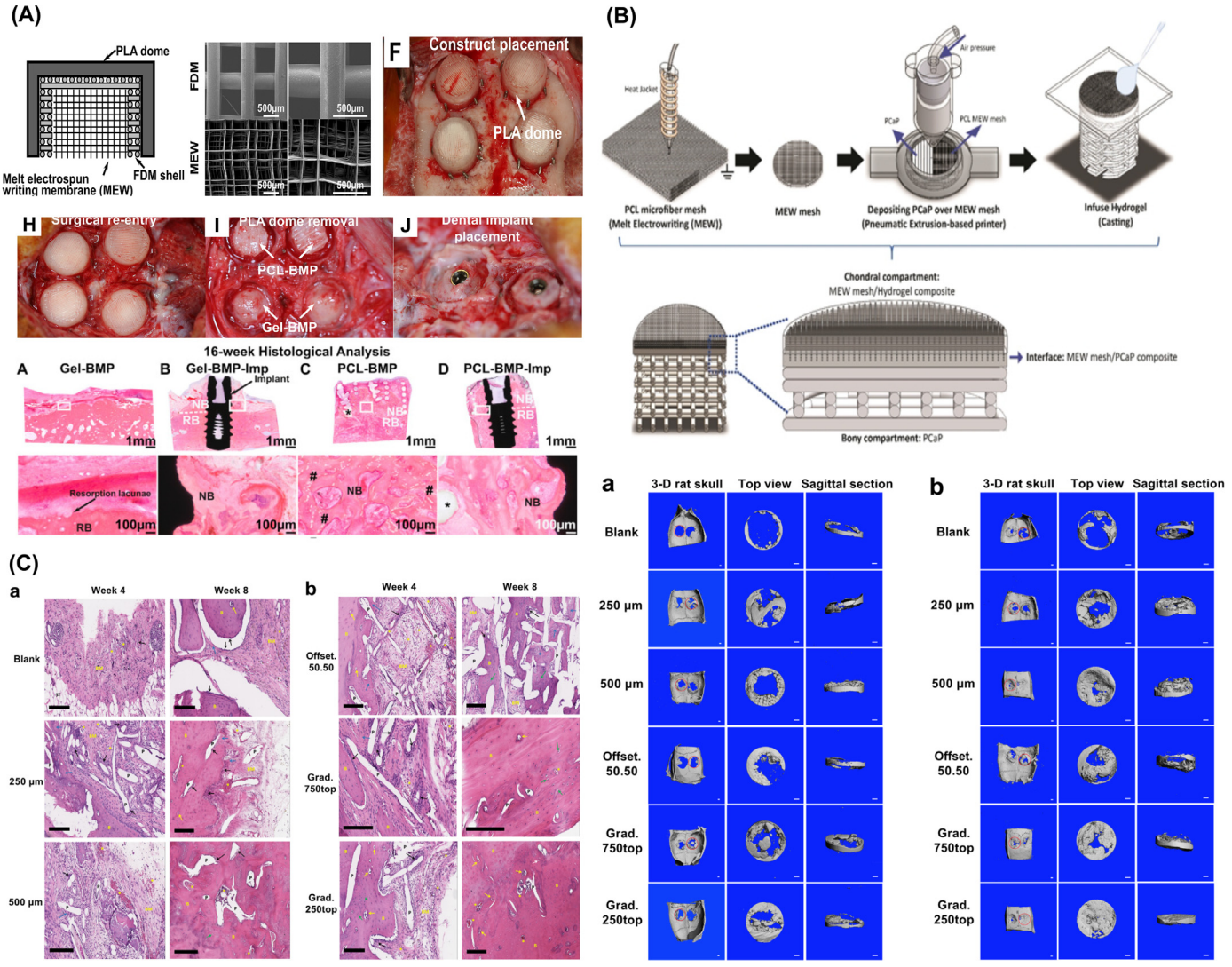

Fig. 7. Multilayered/Multiphasic scaffolds for osteochondral and periodontal regeneration. **(A)** Multiphasic construct for vertical bone augmentation, graphic view of melt electrospun mesh inserted to FDM scaffold and PLLA dome shaped construct and Surgical implantation of constructs onto the sheep calvarium. Adapted from. From Vaquette *et al.* (2021) [70]. **(B)** Schematic illustration of the multiscale osteochondral construct processed via melt writing electrospun fibers reinforced hydrogel-ceramic interfaces. From Diloksumpan *et al.* (2020) [74]. **(C)** Bone regeneration assessment of offset and gradient MEW scaffolds implanted in rat calvarial defects and 3-D reconstructed Micro-CT images showing the degree of bone repair at 4 weeks and 8 weeks post-implantation. From Abbasi *et al.* (2020) [75].

6. Potential applications of MEW scaffolds for DOC tissue regeneration

Despite the striking advances and latest understanding of the impact of MEW in regenerative therapies, the translation of engineering-driven concepts to the clinics relies on a series of biological factors. Next, we discuss how MEW scaffolds interact with different cell types and biomolecules aiming at providing foundational knowledge toward MEW potential in DOC tissue regeneration.

6.1. MEW scaffolds and cell behavior

Many studies have demonstrated that MEW scaffolds can resemble unique features of the native ECM and regulate a high level of cellular events [22,42,80]. It is recognized that cell behavior, in terms of morphology and molecular signaling, is affected by scaffold topography, strand spacing, scaffold laydown patterns and porosity. Cellular orientation is of particular concern in tissues that have a high level of cell alignment. The highly hierarchical organization, of orthopedic and periodontal ligament tissues conveys elasticity and high tensile strength crucial for bearing the physiological cyclic loading during function. The utilization of highly-ordered MEW fibers, for instance, induced spontaneous cell alignment [48]. Aligned fibers were able to orient human mesenchymal stem cells (hMSCs) towards the fiber's direction where that alignment was lost in cells cultured on the other pattern [81]. Likewise, Paxton *et al.* have explored the effect of the laydown angles on cellular behavior; scaffolds with laydown angles of 20° and 50° revealed more uncontrolled cell bridging after 21 days compared to 90° [48]. A laydown of 90° also resulted in cells branching around the corners of each strand and higher yes-associated protein (YAP) expression, whereas less branching was evident at 45° laydown patterns [82]. Moreover, shape-driven pathway is evident to direct cell phenotype commitment by modifying the biophysical characteristics of biomaterial substrates, *e.g.*, small strands spacing may tune construct stiffness and subsequently direct stem cell commitment [52]. A strand spacing of 100 μm increased toughness and yield forces up to 2.8-fold when compared to 200 and 300 µm strands, and was also observed to induce higher nuclear YAP

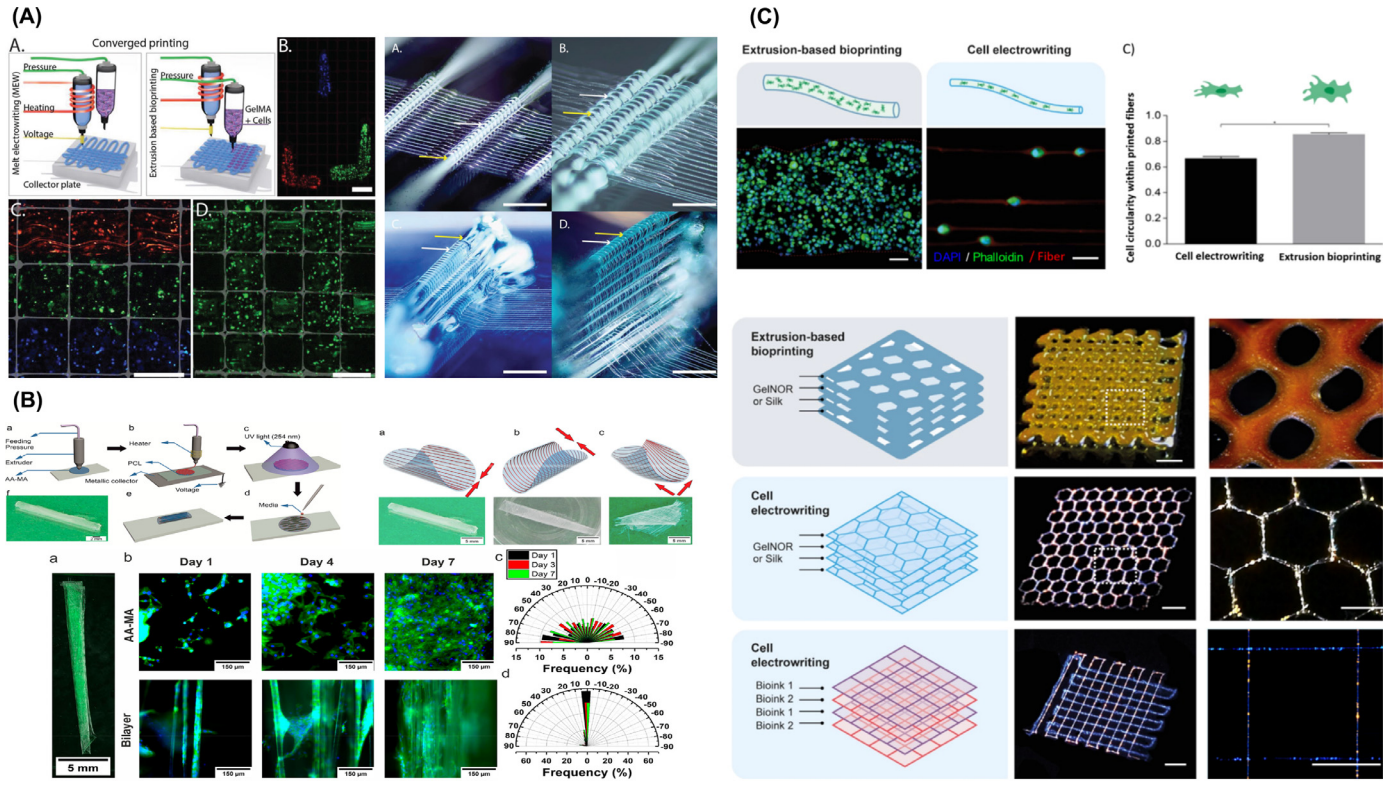

Fig. 8. Multitechnology biofabrication approaches. **(A)** Cell distribution and out-of-plane printing architecture. From Ruijter *et al.* (2019) [77]. **(B)** Bilayer self-folded tube via 3D printing and melt electrowriting (MEW) of PCL fibers on methacrylated alginate (AA-MA) hydrogel, can be folded at different directions direction; parallel, perpendicular or diagonal-wise. The presence of MEW fibers support Myofibroblast orientation to a higher degree not achievable by AA-MA film without fibers. From Constante *et al.* (2021) [78]. **(C)** Cell electrowritten (CEW) fibers on gelnor-based cell-laden scaffolds compared to conventional extrusion bioprinting. Single cells precisely aligned along the pattern in CEW while extrusion-bioprinted fibers had thicker filament of multiple cells distributed homogeneously. CEW allows simultaneous multiple bioinks printing in a single construct. From Castilho *et al.* (2021) [28].

expression and osteogenic commitment of seeded MSCs. Furthermore, heterogenous gradient spacings, improve cell entrapment for an efficient cell scaffold-based therapy for osseous tissue regeneration in the presence of bioactive molecules (*e.g.*, CaP coating) [22]. Altogether, these findings open up new perspectives for potential applications in hard tissue regeneration [82].

One of the main hurdles in the production of biomaterials and 3D scaffolds remains the ability to guide the innate immune response following implantation. A key player in the innate immune system in response to inflammatory conditions and overall inflammatory response at the implantation site, is the conversion of pro-inflammatory (M1) to the anti-inflammatory, pro-healing (M2) type macrophages. In this way, a geometry-controlled scaffold that precisely drives macrophage polarization has tremendous clinical potential. To that end, Tylek *et al.* fabricated box-shaped MEW scaffolds with strand spacings ranging from 100 μm to 40 μm. The 40 μm strand spacing supports human macrophage elongation and spontaneous differentiation as well as upregulation of M2 markers (*e.g.*, CD163, CD206, and IL-10) **(Fig. 9A)** [43]. Relevant to the DOC context, the design of geometry-controlled scaffolds able to amplify tissue regeneration via macrophage polarization while enhancing inflammation resolution would have a significant impact in periodontics, particularly in a pathogen-driven chronic inflammatory disorder such as periodontitis (gum disease). Altogether, biomaterial-informed scaffolds are complementary, if not a potential substitute, for currently employed therapeutic molecules to direct the response of progenitor cells to promote tissue healing and subsequently regeneration of compromised dental, oral, and craniofacial tissues.

6.2. MEW scaffolds as 3D microenvironments to study and regenerate tissues

Because of the continuous growth of elderly population, and the need for treating dental, oral, and craniomaxillofacial defects caused by trauma, diseases and resections, there is a critical need to develop platforms to better understand physiological and pathologic environments to devise more predictable regenerative therapies. For instance, 3D tissue engineered platforms closely mimicking both soft and hard tissue components of oral tissues can offer invaluable *in vitro* models to investigate tissue invasion in head and neck cancer (HNC) and serve as diagnostic and therapeutic tools. HNC such as squamous cell carcinoma (SCC) deliberated one of the poor prognosis malignities that impact overall quality of patient life. Therefore, the establishment of true 3D *in vitro* models to help bridge the gap of available 2D culture models is central to recapitulating the complexity of HNC microenvironment and further help developing improved therapeutic solutions.

To study cases of cancer progression and bone destruction caused by metastasis, Bock (2019) reported on a platform to facilitate learning the biological processes of cancer progression in the bone compartment in a physiological context comparable to native tissue. In this way, MEW technology was utilized to obtain scaffolds capable to accommodate a co-culture system of human preosteoblast (hPOB) and prostate cancer cells. The 3D bone microenvironment was conferred by a calcium phosphate (CaP) coating on the scaffold to elucidate the nature of interactions between cancer cells and osteoblasts, and the biological consequences of androgen suppression on cancer progression in bone [26]. The proposed arti-

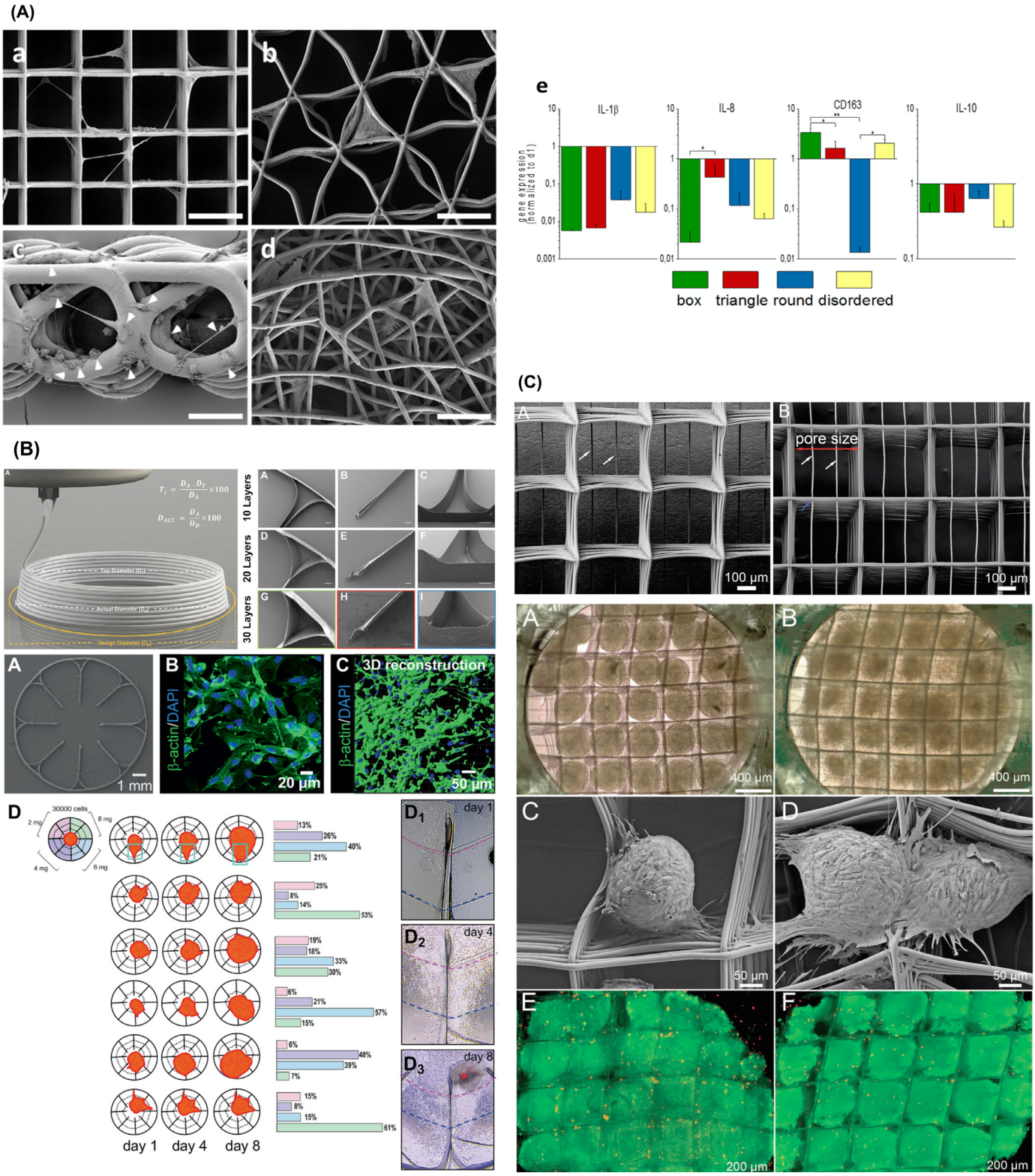

Fig. 9. Current *In vitro* platforms for MEW for studying disease and engineering tissues. **(A)** Macrophages and MEW scaffold interaction suggested spontaneous differentiation of M1 toward the anti-inflammatory type (M2), while both M1-markers, IL-1β and IL-8, were decreased and the M2 markers, CD163 and IL-10, rather increased. From. Tylek *et al.* (2020) [43]. **(B)** Schematic of the MEW circular structure of a 3D *in vitro* radial culture device for glioblastoma cell migration analysis. From Bakirci *et al.* (2020) [84]. **(C)** Adipose stem cells (ASC) spheroids in box-structured MEW scaffolds shows attachment to the fibers and adjacent spheroids. From McMaster *et al.* (2019) [44].

ficial metastatic tissue model holds promise for examining cell–cell and cell–matrix interactions between cancer and bone cells in an actual 3D microenvironment [26].

Likewise, 3D *in vitro* models that resemble the endosteal microenvironment would allow to study treatment modalities of blood and immune-related diseases. Cascante *et al.* established a physiologically relevant 3D microenvironment utilizing MEW to sustain the suitability of placenta-derived mesenchymal stem cells (plMSCs) co-cultured with primary human osteoblasts (hOBs). The endosteal bone-like microenvironment supports the proliferation and migration of primary human hematopoietic stem cells when compared to 2D environment [83]. Another example, a MEW radial construct filled with Matrigel® was conceptualized to investigate glioblastoma cell migration, as a result of matrix concentration and the topographical cues of MEW fibers **(Fig. 9B)** [84]. The reinforced Matrigel with MEW fibers allows the characterization of glycine receptor-transfected cells electrophysiologically in 3D [54].

Over the last few years, other research groups have demonstrated that the design of MEW constructs provided retention and enabled long-term structural integrity to improve differentiation of stem cells (*e.g.*, adipose-derived stromal cell). McMaster *et al.* cultured multicellular spheroids in 360 μm strand spacing box-shaped MEW scaffolds supported by two single catching fibers **(Fig. 9C).** Interestingly, the utilization of MEW scaffolds for the seeding of multicellular spheroids may be readily transferred to engineering cartilage tissue for which pellet culture is frequently used or preseeded endothelial cells prior to spheroid insertion for vascularized, sheet-like structures [44]. Furthermore, MEW provides the ability to scale expansion up for cell-based and immunotherapy. For instance, defined spaces and high surface area of MEW lattice-based scaffolds allows to recapitulate the dynamic interactions of primary human lymphoid tissues and induction of proliferative signals for T cell expansion [85]. Collectively, a deep understanding of the cell and molecular signatures in health and disease conditions affecting DOC tissues is key to designing proper scaffolds, as well as 3D *in vitro* platforms to improve therapeutics potential.

6.3. Rebuilding vascularization and innervation via MEW

DOC tissues present hierarchically organized vascularization and innervation. Moreover, it is not uncommon to observe trauma, or injuries to vessels and nerves due to iatrogenic (*i.e.*, inadvertently induced by the surgeon/dentist) procedures. In regenerative therapies, the vascularization of engineered constructs enhances cell signaling and avoids core necrosis. However, *in vitro* vascularization of biofabricated tissues is challenging due to vascular network geometry, critical for cell survival, metabolic activity and differentiation potential. MEW constructs/scaffolds, combined with a cell-accumulation technique, would allow for the formation of controlled capillary-like network structures [86]. The combination of MEW and electrospinning allowed for the formation of a simultaneous layer-specific native vessel, recapitulated the tunica intima and tunica media, and relevant progenitor cell sources for vascular grafts [87]. Moreover, MEW constructs and cell-based therapies have many applications to produce multiple specialized tissues. Tubular MEW constructs provided an orthotopic platform that mimicked the periosteal microenvironment and a co-cultured system of human endothelial and bone marrow mesenchymal stem cells resembled both the vascular and osteogenic niche of native bone [88].

Similarly, 3D printed neural regeneration strategies have also emerged as new therapeutic approaches for neural diseases/injuries. For instance, the development of cortical neurons in fiber-reinforced matrices demonstrated to be possible to mimic the native embryonic brain environment, thus laying the groundwork for studying the neuronal cells network in a 3D environment under normal and pathophysiological conditions [89]. From a dental perspective, further insights in the field would favor the development of strategies to recover micro-innervation and proprioception of the dental pulp after necrosis, and the regeneration of damaged nerves or chronic paresthesia after trauma, resection, or iatrogenic dental procedures.

6.4. MEW-based scaffolds for regeneration of DOC tissues and interfaces

Craniomaxillofacial bones and connective tissues organization are complex in size, confinement, and function, compared to other regions in the human body. Strategies to regenerate dentin microtubular structure lost by caries, or the intimate interaction among disc, ligaments, and craniomandibular bones in the TMJ remain elusive. Nonetheless, as previously mentioned in this review, the freedom of design and resolution of MEW scaffolds can guide future strategies for tooth and TMJ regeneration. For example, a biphasic construct was fabricated to replicate bone-ligament-bone (BLB) interfaces simulating the native anterior cruciate ligament (ACL) organization [81]. The specific geometries of the construct influence cell orientation and growth, while the mechanical performance at the interface is a key feature to improve tensile properties and provide strong anchoring of ligament to bone. These approaches can further direct BLB interfaces regeneration in the craniomaxillofacial region [81].

Current insights on MEW and hydrogels combination may lead to the fabrication of bioengineered constructs mimicking the structure, and native mechanical and biological behavior of the TMJ. Functionalized hydrogels delivering biomolecules (*e.g.*, bone morphogenetic protein-2) combined with biphasic FDM and MEW scaffolds replicating both cancellous and cortical bone have been reported [69]. Alternatively, hard-to-soft tissue interfaces reconstruction, through MEW and hydrogels combination, emulates viscoelasticity and stress relaxation behavior of cartilage and ligaments, in response to mechanical loading [64,65]. Nonetheless, the highest complexity in DOC tissues is probably in the periodontium – alveolar bone, cementum, periodontal ligament, and gingiva – working as a single complex system with supportive, protective, and proprioceptive functions [3]. To date, the clinical management of the tissue destruction caused by periodontitis has encompassed scaling and root planing, flap surgery, biologics (*e.g.,* enamel matrix derivative, EMD), bone grafting, and guided tissue regeneration (GTR) based on the utility of a biodegradable membrane that, while acting as a physical barrier against soft tissue invagination, encourages resident progenitor cells to stimulate periodontal regeneration. Nonetheless, though current treatments can promote some level of tissue regeneration, the reduced predictability and efficacy in situations of severe tissue destruction call for improved approaches that can better mimic the multi-tissue complexity and 3D architecture of periodontal defects. Currently, there is no clinically available technology that offers the opportunity to create personalized scaffolds to predictably address regeneration of the periodontal attachment apparatus on root surfaces with severe bone loss. It is, therefore, well understood that highly complex defects impair the quality and amount of vascular and cellular elements, and, by consequence, are less favorable for the success of a regenerative strategy [90]. In this sense, mimicking the complexity of the periodontal individual compartments and interconnectivity stand as the most critical issue regarding scaffold-based periodontal regeneration [4].

Fortunately, the advent of MEW, in combination with complementary 3D (bio)printed regenerative approaches, has arisen as a unique technology to generate scaffolds/constructs mimicking highly-complex and organized structures that can be translated to study and regenerate bone and cartilage in the craniofacial

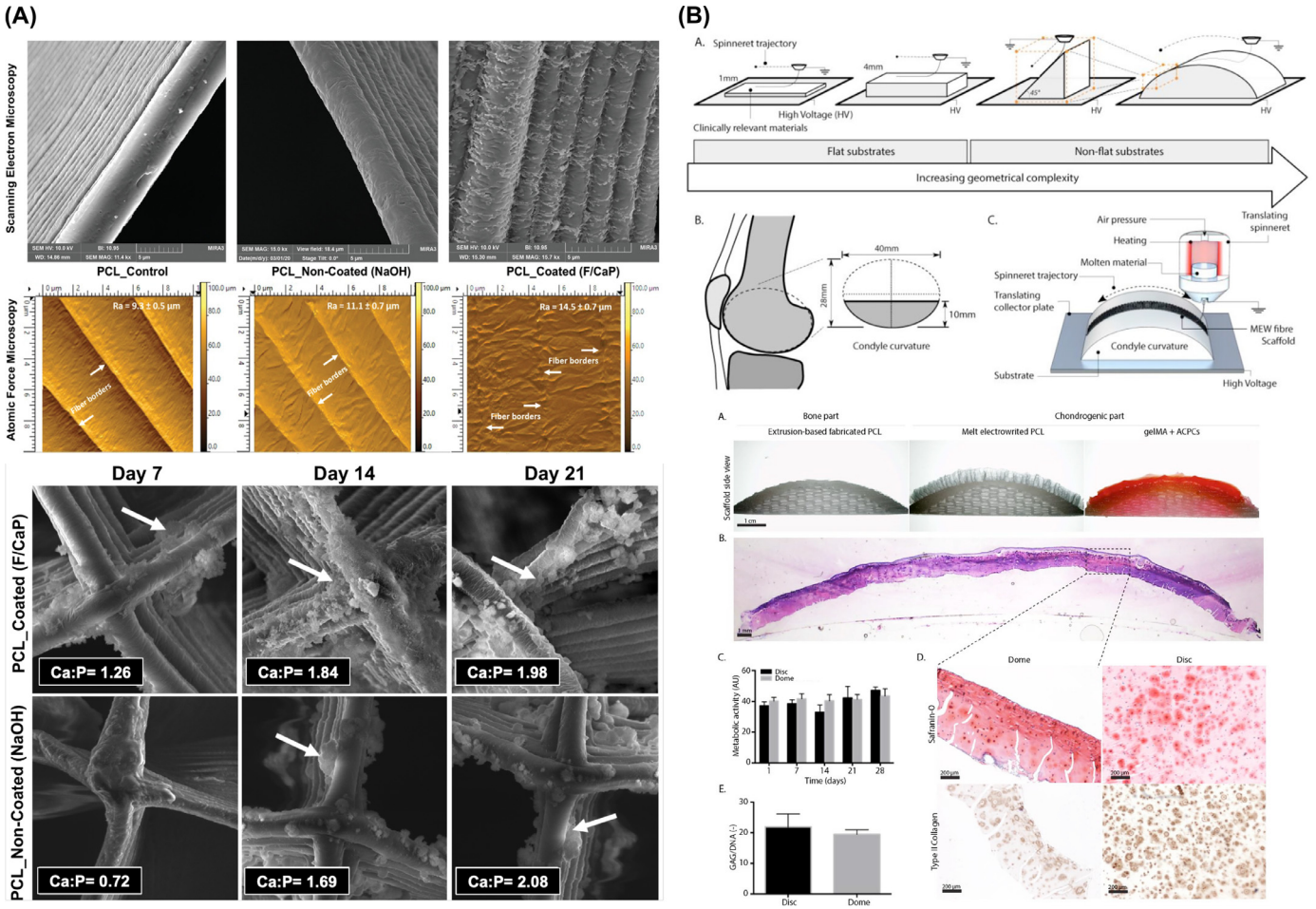

Fig. 10. Tissue-specific scaffolds/constructs that direct stem cells differentiation and mimic the biomechanics of the tissue to be regenerated. **(A)** F/CaP scaffold exhibited distinct surface texture and bioactivity when immersed in SBF. From Daghrery *et al.* (2021) [27]. **(B)** Non flat geometries via resurfacing PCL to mimicking the contour of a human femoral condyle surface, enables cartilage-like tissue formation. From Peiffer et al. (2021) [25].

region. MEW allows the synthesis of multiphasic, site-specific or non-flat anatomically relevant designs that can be applied for different tissues and interfaces **(Fig. 10A-B)** [25]. These concepts have been initially translated for periodontal regeneration, where a multilayer membrane, fabricated by MEW, provided an optimal substrate for tissue growth and, at the same time, acted as a barrier against soft-tissue cells invagination and microorganisms transmigration [51]. Moreover, combining MEW with other techniques address structural compartmentalization of both hard and soft tissues [71]. For example, converging MEW and traditional electrospinning, with bone marrow-derived mesenchymal stem cells and periodontal ligament stem cell sheets, fostered bone and periodontal ligament regeneration [71]. Additionally, biphasic membranes combining FDM-CaP, for bone compartment, and MEW for PDL compartment, showed improved interconnectivity between the bone and periodontal ligament compartments in *in vivo* subcutaneously implanted dentin slice's model [68].

More recently, our group reported on the fabrication of tissue-specific scaffolds for periodontal tissue regeneration via MEW and the development of a novel nanocoating approach **(Fig. 10A)**. The innovative and unique nanostructured fluorinated calcium phosphate (F/CaP) coating led to periodontal tissue regeneration while supporting periodontal ligament formation when implanted in a well-established periodontal defect model in rats **(Fig. 11A)**. The results of that investigation demonstrated that ability of MEW to generate personalized constructs able to encourage tissue-specific differentiation of progenitor cells, and ultimately the regeneration of soft and hard periodontal tissues, while affording antimicrobial action **(Fig. 11B)**. To that end, the advantages associated with MEW and the opportunities to integrating this promising AM tool with well-established 3D (bio)printing technologies represent a clear path to the translation of scaffolds that replicate not only the micron-scale, but also the complex 3D geometries of periodontal defects.

7. Conclusion and future perspectives

Recapitulating hierarchical organization, along with the biological and mechanical behavior of hard and soft tissues and interfaces, is the ultimate goal of tissue regeneration. To date, a plethora of AM technologies have been used to synthesize scaffolds for application in regenerative dental medicine, and this review focused on the emergence of MEW as a relevant strategy to build scaffolds/constructs with freedom of design and accuracy, while recapitulating native tissues' arrangement. In the same way, MEW allows the combination with other AM tools to fabricate hybrid scaffolds that address tissue complexity, biological, and physical properties. Although MEW is a promising technology that aids in replicating the nature, size, and organization of tissues, the full possibilities of this fairly novel approach in the biofabrication of dental, oral, and craniofacial (DOC) structures continue to be unveiled.

As control over the technology moves forward, it is possible to design scaffolds that address major concerns related to the regeneration of DOC tissues, such as the 3D complexity of periodontal

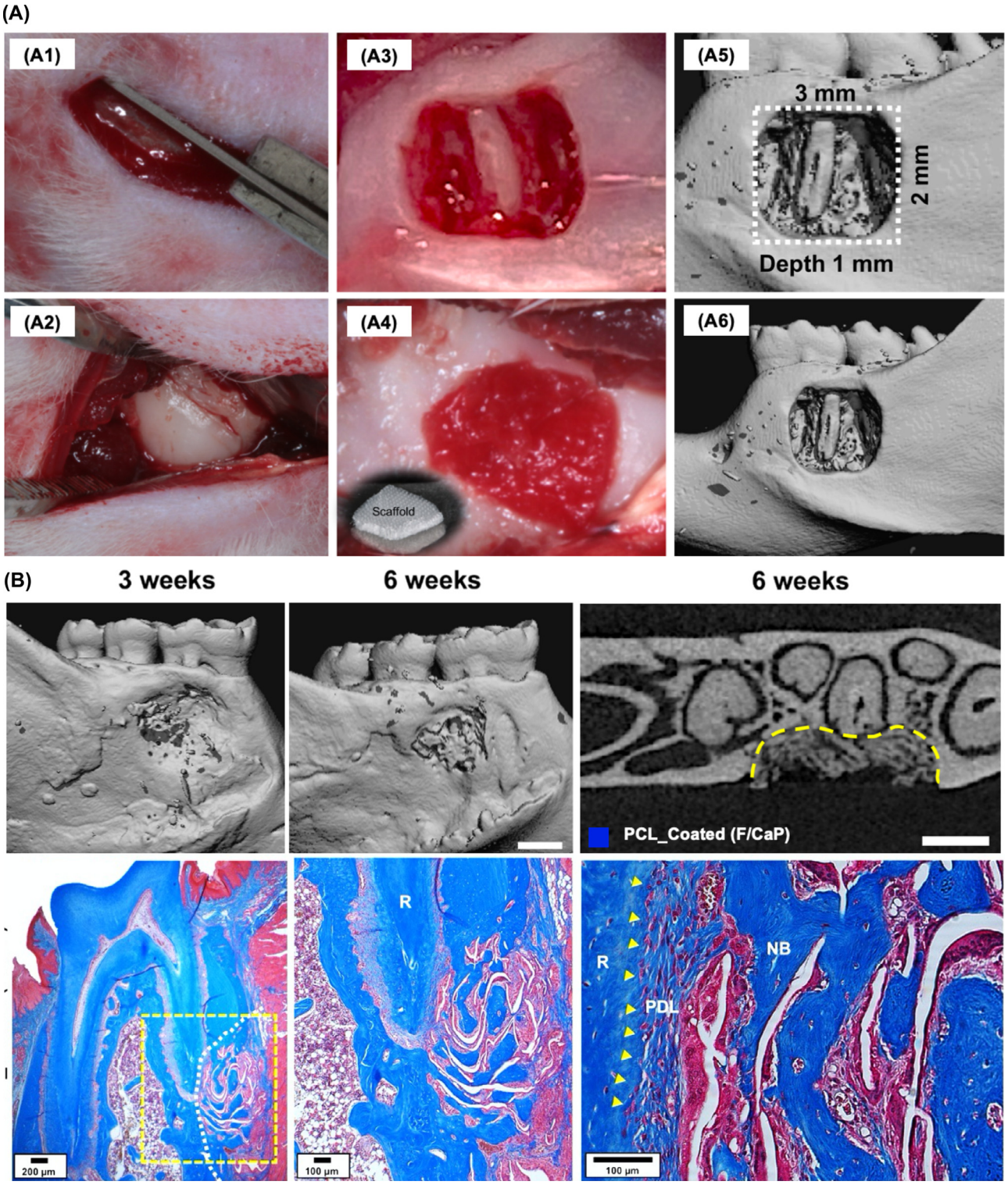

Fig. 11. Highly-Ordered, nanostructured fluorinated cap-coated melt electrowritten scaffold for periodontal regeneration **(A)** Generation and characterization of rat mandibular periodontal fenestration defect model. **(B)** Micro-CT assessments and MT-stained indicated neotissue formation and Sharpey's fiber insertions to new bone and cementum formation after 6 weeks post-implantation of MEW-F/CaP scaffold. From Daghrery *et al.* (2021) [27].

defects, mechanical and biological behavior of the TMJ, and permanent damage due to chronic diseases, trauma, and resectioning. By taming all the possibilities discussed in this review, and selecting the proper combination of materials, biomolecules, and cells; MEW provides unique conditions to create highly complex constructs/scaffolds with supportive biophysical properties to reconstruct damaged DOC tissues. Moreover, MEW scaffolds' ability to recapitulate hard-to-soft tissue transitions fosters the development of site-specific constructs for alveolar bone, TMJ, and periodontal tissue regeneration.

The applicability of MEW to precisely fabricate compartmentalized scaffolds, control over an infinite range of geometries, and recently proposed cell electrowriting (CEW) that expands MEW into the direct writing of living cells, form a strong foundation for fu-

ture work on cellular microenvironments and immediate cell commitment in multicellular tissue constructs. Furthermore, current studies that use MEW scaffolds for bone and connective tissues' regeneration, and possible integration with vessels and neural functionality, direct the steps towards developing tissue-specific scaffolds. These aspects are truly valuable when they mimic anatomical and functional tissue-specificity while printing scaffolds to regenerate the pulp-dentin complex and periodontal tissues with their respective delicate interfaces, while also providing a better understanding of the aspects involved in head and neck tumor progression.

Lastly, opportunities related to the convergence of MEW with other 3D (bio)printing tools, or other complementary fabrication technologies such as plasma technologies or acoustic levitation, address specific response challenges for multi-tissue regeneration. In this sense, constant improvements in the printability of high-resolution image-based scaffolds encourage work on micro- and nano-scale complex designs using converged AM technologies. It is expected that these improved scaffolds can hierarchically mimic the ECM of native tissues and have control over the profile that guides future defect-specific, single-step scaffolds for DOC tissues and tissue interfaces, and thus expedite its clinical translation.

Declaration of Competing Interest

The authors declare no competing financial interest or with respect to the authorship and/or publication of this article.

Acknowledgements

The graphical abstract and Fig. 1 presented in this manuscript were created with BioRender.com. The authors are also grateful for the cartoons designed by Kenneth Rieger (Multimedia Designer, Department, School of Dentistry, University of Michigan, Ann Arbor, MI, USA). This project was supported by funding from the National Institutes of Health (NIH, National Institute of Dental and Craniofacial Research [K08DE023552 and R01DE026578 to MCB] and National Institute of General Medical Sciences [R01GM143938 to MCB]), the Osteology Foundation (Advanced Researcher Award), OsteoScience Foundation (Peter Geistlich Research Award), the International Association for Dental Research (IADR-GSK Innovation in Oral Care Award and IADR-AO Implant Sciences Award), the American Academy of Implant Dentistry Foundation, the European Union H2020 program BRAVƎ (grant number 874827), the Gravitation Program "Materials Driven Regeneration" (024.003.013) and the Reprint project (OCENW.XS5.161) by the Netherlands Organization for Scientific Research

References

[1] V. Petrovic, P. Zivkovic, D. Petrovic, V. Stefanovic, Craniofacial bone tissue engineering, Oral Surg. Oral Med. Oral Pathol. Oral Radiol. 114 (2012) e1–e9.
[2] R. Dwivedi, S. Kumar, R. Pandey, A. Mahajan, D. Nandana, D.S. Katti, D. Mehrotra, Polycaprolactone as biomaterial for bone scaffolds: Review of literature, J. Oral Biol. Craniofac. Res. 10 (2020) 381–388.
[3] M.C. Bottino, V. Thomas, G. Schmidt, Y.K. Vohra, T.-M.G. Chu, M.J. Kowolik, G.M. Janowski, Recent advances in the development of GTR/GBR membranes for periodontal regeneration–a materials perspective, Dent. Mater. 28 (2012) 703–721.
[4] Z. Aytac, N. Dubey, A. Daghrery, J.A. Ferreira, I.J. de S. Araújo, M. Castilho, J. Malda, M.C. Bottino, Innovations in craniofacial bone and periodontal tissue engineering – from electrospinning to converged biofabrication, Int. Mater. Rev. (2021) 1–38.
[5] Y. Du, J.L. Guo, J. Wang, A.G. Mikos, S. Zhang, Hierarchically designed bone scaffolds: From internal cues to external stimuli, Biomaterials 218 (2019) 119334.
[6] A. Daghrery, Z. Aytac, N. Dubey, L. Mei, A. Schwendeman, M.C. Bottino, Electrospinning of dexamethasone/cyclodextrin inclusion complex polymer fibers for dental pulp therapy, Colloids Surf. B (2020) 111011.
[7] N. Dubey, J.A. Ferreira, A. Daghrery, Z. Aytac, J. Malda, S.B. Bhaduri, M.C. Bottino, Highly tunable bioactive fiber-reinforced hydrogel for guided bone regeneration, Acta Biomater. (2020).
[8] G. Hochleitner, T. Jüngst, T.D. Brown, K. Hahn, C. Moseke, F. Jakob, P.D. Dalton, J. Groll, Additive manufacturing of scaffolds with sub-micron filaments via melt electrospinning writing, Biofabrication 7 (2015) 035002.
[9] J. Zhiwei, B. Luo, S. Xiang, H. Ma, Y. Yu, W. Yang, 3D printing of HA /PCL composite tissue engineering scaffolds, Adv. Indust. Eng. Polym. Res. 2 (2019).
[10] O. Bas, D. D'Angella, J.G. Baldwin, N.J. Castro, F.M. Wunner, N.T. Saidy, S. Kollmannsberger, A. Reali, E. Rank, E.M. De-Juan-Pardo, D.W. Hutmacher, An Integrated Design, Material, and Fabrication Platform for Engineering Biomechanically and Biologically Functional Soft Tissues, ACS Appl. Mater. Interfaces 9 (2017) 29430–29437.
[11] M. Castilho, M. de Ruijter, S. Beirne, C.C. Villette, K. Ito, G.G. Wallace, J. Malda, Multitechnology Biofabrication: A New Approach for the Manufacturing of Functional Tissue Structures? Trends Biotechnol. 38 (2020) 1316–1328.
[12] I. Ozbolat, H. Gudapati, A review on design for bioprinting, Bioprinting 3–4 (2016) 1–14.
[13] A. Boccaccio, A.E. Uva, M. Fiorentino, L. Lamberti, G. Monno, A Mechanobiology-based Algorithm to Optimize the Microstructure Geometry of Bone Tissue Scaffolds, Int. J. Biol. Sci. 12 (2016) 1–17.
[14] M. Castilho, M. Dias, U. Gbureck, J. Groll, P. Fernandes, I. Pires, B. Gouveia, J. Rodrigues, E. Vorndran, Fabrication of computationally designed scaffolds by low temperature 3D printing, Biofabrication 5 (2013) 035012.
[15] K.-H. Huang, Y.-H. Lin, M.-Y. Shie, C.-P. Lin, Effects of bone morphogenic protein-2 loaded on the 3D-printed MesoCS scaffolds, J. Formos. Med. Assoc. 117 (2018) 879–887.
[16] D.W. Hutmacher, T. Schantz, I. Zein, K.W. Ng, S.H. Teoh, K.C. Tan, Mechanical properties and cell cultural response of polycaprolactone scaffolds designed and fabricated via fused deposition modeling, J. Biomed. Mater. Res. 55 (2001) 203–216.
[17] H. Chen, A. de B.F.B. Malheiro, C. van Blitterswijk, C. Mota, P.A. Wieringa, L. Moroni, Direct Writing Electrospinning of Scaffolds with Multidimensional Fiber Architecture for Hierarchical Tissue Engineering, ACS Appl. Mater. Interfaces 9 (2017) 38187–38200.
[18] T.M. Robinson, D.W. Hutmacher, P.D. Dalton, The Next Frontier in Melt Electrospinning: Taming the Jet, Adv. Funct. Mater. 29 (2019) 1904664.
[19] E. McColl, J. Groll, T. Jungst, P.D. Dalton, Design and fabrication of melt electrowritten tubes using intuitive software, Mater. Des. 155 (2018) 46–58.
[20] A.M. van Genderen, K. Jansen, M. Kristen, J. van Duijn, Y. Li, C.C.L. Schuurmans, J. Malda, T. Vermonden, J. Jansen, R. Masereeuw, M. Castilho, Topographic Guidance in Melt-Electrowritten Tubular Scaffolds Enhances Engineered Kidney Tubule Performance, BioRxiv. (2020) 2020.09.16.300004.
[21] M. Castilho, D. Feyen, M. Flandes-Iparraguirre, G. Hochleitner, J. Groll, P.A.F. Doevendans, T. Vermonden, K. Ito, J.P.G. Sluijter, J. Malda, Melt Electrospinning Writing of Poly-Hydroxymethylglycolide-co-ε-Caprolactone-Based Scaffolds for Cardiac Tissue Engineering, Adv. Healthc. Mater. 6 (2017).
[22] N. Abbasi, A. Abdal-hay, S. Hamlet, E. Graham, S. Ivanovski, Effects of Gradient and Offset Architectures on the Mechanical and Biological Properties of 3-D Melt Electrowritten (MEW) Scaffolds, ACS Biomater. Sci. Eng. 5 (2019) 3448–3461.
[23] C. Großhaus, E. Bakirci, M. Berthel, A. Hrynevich, J.C. Kade, G. Hochleitner, J. Groll, P.D. Dalton, Melt Electrospinning of Nanofibers from Medical-Grade Poly(ε-Caprolactone) with a Modified Nozzle, Small 16 (2020) 2003471.
[24] I. Liashenko, A. Hrynevich, P.D. Dalton, Designing Outside the Box: Unlocking the Geometric Freedom of Melt Electrowriting using Microscale Layer Shifting, Adv. Mater. 32 (2020) 2001874.
[25] Q.C. Peiffer, M. de Ruijter, J. van Duijn, D. Crottet, E. Dominic, J. Malda, M. Castilho, Melt electrowriting onto anatomically relevant biodegradable substrates: Resurfacing a diarthrodial joint, Mater. Des. 195 (2020) 109025.
[26] N. Bock, Bioengineered Microtissue Models of the Human Bone Metastatic Microenvironment: A Novel In Vitro Theranostics Platform for Cancer Research, Methods Mol. Biol. 2054 (2019) 23–57.
[27] A. Daghrery, J.A. Ferreira, I.J. de Souza Araújo, B.H. Clarkson, G.J. Eckert, S.B. Bhaduri, J. Malda, M.C. Bottino, A Highly Ordered, Nanostructured Fluorinated CaP-Coated Melt Electrowritten Scaffold for Periodontal Tissue Regeneration, Adv. Healthc. Mater. (2021) e2101152.
[28] M. Castilho, R. Levato, P.N. Bernal, M. de Ruijter, C.Y. Sheng, J. van Duijn, S. Piluso, K. Ito, J. Malda, Hydrogel-Based Bioinks for Cell Electrowriting of Well-Organized Living Structures with Micrometer-Scale Resolution, Biomacromolecules (2021).
[29] T.D. Brown, P.D. Dalton, D.W. Hutmacher, Direct Writing By Way of Melt Electrospinning, Adv. Mater. 23 (2011) 5651–5657.
[30] J.N. Haigh, T.R. Dargaville, P.D. Dalton, Additive manufacturing with polypropylene microfibers, Mater. Sci. Eng. C 77 (2017) 883–887.
[31] F. Chen, G. Hochleitner, T. Woodfield, J. Groll, P.D. Dalton, B.G. Amsden, Additive Manufacturing of a Photo-Cross-Linkable Polymer via Direct Melt Electrospinning Writing for Producing High Strength Structures, Biomacromolecules 17 (2016) 208–214.
[32] J.N. Haigh, Y. Chuang, B. Farrugia, R. Hoogenboom, P.D. Dalton, T.R. Dargaville, Hierarchically Structured Porous Poly(2-oxazoline) Hydrogels, Macromol. Rapid Commun. 37 (2016) 93–99.
[33] G. Hochleitner, E. Fürsattel, R. Giesa, J. Groll, H.-W. Schmidt, P.D. Dalton, Melt Electrowriting of Thermoplastic Elastomers, Macromol. Rapid Commun. 39 (2018) 1800055.
[34] R.S. Diaz, J.-R. Park, L.L. Rodrigues, P.D. Dalton, E.M. De-Juan-Pardo, T.R. Dargaville, Highly Elastic Scaffolds Produced by Melt Electrowriting of Poly(L-lactide-co-ε-caprolactone), Adv. Mater. Tech. (2021) 2100508 n/an.d..
[35] A. Hrynevich, B.Ş. Elçi, J.N. Haigh, R. McMaster, A. Youssef, C. Blum, T. Blunk,

G. Hochleitner, J. Groll, P.D. Dalton, Dimension-Based Design of Melt Electrowritten Scaffolds, Small 14 (2018) 1800232.
[36] M.L. Muerza-Cascante, D. Haylock, D.W. Hutmacher, P.D. Dalton, Melt electrospinning and its technologization in tissue engineering, Tissue Eng. Part B Rev. 21 (2015) 187–202.
[37] F.M. Wunner, P. Mieszczanek, O. Bas, S. Eggert, J. Maartens, P.D. Dalton, E.M. De-Juan-Pardo, D.W. Hutmacher, Printomics: the high-throughput analysis of printing parameters applied to melt electrowriting, Biofabrication 11 (2019) 025004.
[38] A. Daneshfar, S.L. Edwards, L.F. Dumée, L. Kong, T.C. Hughes, Predicting Operating Rules for Successful Melt Electrowriting, ACS Appl. Polym. Mater. 3 (2021) 1890–1898.
[39] F. Wunner, O. Bas, N. Saidy, P. Dalton, E. De Juan-Pardo, D. Hutmacher, Melt Electrospinning Writing of Three-dimensional Poly(ε-caprolactone) Scaffolds with Controllable Morphologies for Tissue Engineering Applications, J. Visual. Exp. (2017) 2017.
[40] F.M. Wunner, M.-L. Wille, T.G. Noonan, O. Bas, P.D. Dalton, E.M. De-Juan–Pardo, D.W. Hutmacher, Melt Electrospinning Writing of Highly Ordered Large Volume Scaffold Architectures, Adv. Mater. 30 (2018) 1706570.
[41] M. Castilho, A. van Mil, M. Maher, C.H.G. Metz, G. Hochleitner, J. Groll, P.A. Doevendans, K. Ito, J.P.G. Sluijter, J. Malda, Melt Electrowriting Allows Tailored Microstructural and Mechanical Design of Scaffolds to Advance Functional Human Myocardial Tissue Formation, Adv. Funct. Mater. 28 (2018) 1803151.
[42] N. Abbasi, S. Ivanovski, K. Gulati, R.M. Love, S. Hamlet, Role of offset and gradient architectures of 3-D melt electrowritten scaffold on differentiation and mineralization of osteoblasts, Biomater. Res. 24 (2020) 2.
[43] T. Tylek, C. Blum, A. Hrynevich, K. Schlegelmilch, T. Schilling, P.D. Dalton, J. Groll, Precisely defined fiber scaffolds with 40 μm porosity induce elongation driven M2-like polarization of human macrophages, Biofabrication 12 (2020) 025007.
[44] R. McMaster, C. Hoefner, A. Hrynevich, C. Blum, M. Wiesner, K. Wittmann, T.R. Dargaville, P. Bauer-Kreisel, J. Groll, P.D. Dalton, T. Blunk, Tailored Melt Electrowritten Scaffolds for the Generation of Sheet-Like Tissue Constructs from Multicellular Spheroids, Adv. Healthc. Mater. 8 (2019) 1801326.
[45] N.T. Saidy, F. Wolf, O. Bas, H. Keijdener, D.W. Hutmacher, P. Mela, E.M. De-Juan-Pardo, Biologically Inspired Scaffolds for Heart Valve Tissue Engineering via Melt Electrowriting, Small 15 (2019) 1900873.
[46] K. Somszor, O. Bas, F. Karimi, T. Shabab, N.T. Saidy, A.J. O'Connor, A.V. Ellis, D. Hutmacher, D.E. Heath, Personalized, Mechanically Strong, and Biodegradable Coronary Artery Stents via Melt Electrowriting, ACS Macro Lett. (2020) 1732–1739.
[47] T.D. Brown, F. Edin, N. Detta, A.D. Skelton, D.W. Hutmacher, P.D. Dalton, Melt electrospinning of poly(ε-caprolactone) scaffolds: Phenomenological observations associated with collection and direct writing, Mater. Sci. Eng. C 45 (2014) 698–708.
[48] N.C. Paxton, M. Lanaro, A. Bo, N. Crooks, M.T. Ross, N. Green, K. Tetsworth, M.C. Allenby, Y. Gu, C.S. Wong, S.K. Powell, M.A. Woodruff, Design tools for patient specific and highly controlled melt electrowritten scaffolds, J. Mech. Behav. Biomed. Mater. 105 (2020) 103695.
[49] C. Xie, Q. Gao, P. Wang, L. Shao, H. Yuan, J. Fu, W. Chen, Y. He, Structure-induced cell growth by 3D printing of heterogeneous scaffolds with ultrafine fibers, Mater. Des. 181 (2019) 108092.
[50] A. Fuchs, A. Youssef, A. Seher, G. Hochleitner, P.D. Dalton, S. Hartmann, R.C. Brands, U.D.A. Müller-Richter, C. Linz, Medical-grade polycaprolactone scaffolds made by melt electrospinning writing for oral bone regeneration – a pilot study in vitro, BMC Oral Health 19 (2019).
[51] A. Fuchs, A. Youssef, A. Seher, S. Hartmann, R.C. Brands, U.D.A. Müller-Richter, A.C. Kübler, C. Linz, A new multilayered membrane for tissue engineering of oral hard- and soft tissue by means of melt electrospinning writing and film casting – An in vitro study, J. Cranio-Maxillofac. Surg. 47 (2019) 695–703.
[52] C.M. Brennan, K.F. Eichholz, D.A. Hoey, The effect of pore size within fibrous scaffolds fabricated using melt electrowriting on human bone marrow stem cell osteogenesis, Biomed. Mater. 14 (2019) 065016.
[53] P.B. Warren, Z.G. Davis, M.B. Fisher, Parametric control of fiber morphology and tensile mechanics in scaffolds with high aspect ratio geometry produced via melt electrowriting for musculoskeletal soft tissue engineering, J. Mech. Behav. Biomed. Mater. 99 (2019) 153–160.
[54] N. Schaefer, D. Janzen, E. Bakirci, A. Hrynevich, P.D. Dalton, C. Villmann, 3D Electrophysiological Measurements on Cells Embedded within Fiber-Reinforced Matrigel, Adv. Healthc. Mater. 8 (2019) e1801226.
[55] G. Hochleitner, F. Chen, C. Blum, P.D. Dalton, B. Amsden, J. Groll, Melt electrowriting below the critical translation speed to fabricate crimped elastomer scaffolds with non-linear extension behaviour mimicking that of ligaments and tendons, Acta Biomater. 72 (2018) 110–120.
[56] D. Olvera, M.S. Molina, G. Hendy, M.G. Monaghan, Electroconductive Melt Electrowritten Patches Matching the Mechanical Anisotropy of Human Myocardium, Adv. Funct. Mater. 30 (2020) 1909880.
[57] N.T. Saidy, T. Shabab, O. Bas, D.M. Rojas-González, M. Menne, T. Henry, D.W. Hutmacher, P. Mela, E.M. De-Juan-Pardo, Melt Electrowriting of Complex 3D Anatomically Relevant Scaffolds, Front. Bioeng. Biotechnol. 8 (2020).
[58] P. Mieszczanek, T.M. Robinson, P.D. Dalton, D.W. Hutmacher, Convergence of Machine Vision and Melt Electrowriting, Adv. Mater. 33 (2021) 2100519.
[59] I. Liashenko, J. Rosell-Llompart, A. Cabot, Ultrafast 3D printing with submicrometer features using electrostatic jet deflection, Nat. Commun. 11 (2020) 753.
[60] C.D. O'Connell, O. Bridges, C. Everett, N. Antill-O'Brien, C. Onofrillo, C.D. Bella, Electrostatic Distortion of Melt-Electrowritten Patterns by 3D Objects: Quantification, Modeling, and Toolpath Correction, Adv. Mater. Tech. (2021) 2100345 n/a (n.d.).
[61] N.C. Paxton, R. Daley, D.P. Forrestal, M.C. Allenby, M.A. Woodruff, Auxetic tubular scaffolds via melt electrowriting, Mater. Des. 193 (2020) 108787.
[62] O. WICHTERLE, D. LÍM, Hydrophilic Gels for Biological Use, Nature 185 (1960) 117–118.
[63] N.A. Peppas, J.Z. Hilt, A. Khademhosseini, R. Langer, Hydrogels in Biology and Medicine: From Molecular Principles to Bionanotechnology, Adv. Mater. 18 (2006) 1345–1360.
[64] J. Visser, F.P.W. Melchels, J.E. Jeon, E.M. van Bussel, L.S. Kimpton, H.M. Byrne, W.J.A. Dhert, P.D. Dalton, D.W. Hutmacher, J. Malda, Reinforcement of hydrogels using three-dimensionally printed microfibres, Nat. Commun. 6 (2015) 1–10.
[65] O. Bas, E.M. De-Juan-Pardo, C. Meinert, D. D'Angella, J.G. Baldwin, L.J. Bray, R.M. Wellard, S. Kollmannsberger, E. Rank, C. Werner, T.J. Klein, I. Catelas, D.W. Hutmacher, Biofabricated soft network composites for cartilage tissue engineering, Biofabrication 9 (2017) 025014.
[66] M. Castilho, G. Hochleitner, W. Wilson, B. van Rietbergen, P.D. Dalton, J. Groll, J. Malda, K. Ito, Mechanical behavior of a soft hydrogel reinforced with three-dimensional printed microfibre scaffolds, Sci. Rep. 8 (2018) 1–10.
[67] M. de Ruijter, A. Hrynevich, J.N. Haigh, G. Hochleitner, M. Castilho, J. Groll, J. Malda, P.D. Dalton, Out-of-Plane 3D-Printed Microfibers Improve the Shear Properties of Hydrogel Composites, Small 14 (2018) 1702773.
[68] P.F. Costa, C. Vaquette, Q. Zhang, R.L. Reis, S. Ivanovski, D.W. Hutmacher, Advanced tissue engineering scaffold design for regeneration of the complex hierarchical periodontal structure, J. Clin. Periodontol. 41 (2014) 283–294.
[69] P.T. Sudheesh Kumar, S. Hashimi, S. Saifzadeh, S. Ivanovski, C. Vaquette, Additively manufactured biphasic construct loaded with BMP-2 for vertical bone regeneration: A pilot study in rabbit, Mater. Sci. Eng. C Mater. Biol. Appl. 92 (2018) 554–564.
[70] C. Vaquette, J. Mitchell, T. Fernandez-Medina, S. Kumar, S. Ivanovski, Resorbable additively manufactured scaffold imparts dimensional stability to extraskeletally regenerated bone, Biomaterials 269 (2021) 120671.
[71] C. Vaquette, S. Saifzadeh, A. Farag, D.W. Hutmacher, S. Ivanovski, Periodontal Tissue Engineering with a Multiphasic Construct and Cell Sheets, J. Dent. Res. 98 (2019) 673–681.
[72] P.D. Dalton, T.B.F. Woodfield, V. Mironov, J. Groll, Advances in Hybrid Fabrication toward Hierarchical Tissue Constructs, Adv. Sci. 7 (2020) 1902953.
[73] M. Castilho, V. Mouser, M. Chen, J. Malda, K. Ito, Bi-layered micro-fibre reinforced hydrogels for articular cartilage regeneration, Acta Biomater. 95 (2019) 297–306.
[74] P. Diloksumpan, M. de Ruijter, M. Castilho, U. Gbureck, T. Vermonden, P.R. van Weeren, J. Malda, R. Levato, Combining multi-scale 3D printing technologies to engineer reinforced hydrogel-ceramic interfaces, Biofabrication 12 (2020) 025014.
[75] N. Abbasi, R.S.B. Lee, S. Ivanovski, R.M. Love, S. Hamlet, In vivo bone regeneration assessment of offset and gradient melt electrowritten (MEW) PCL scaffolds, Biomater. Res. 24 (2020) 17.
[76] O. Bas, S. Lucarotti, D.D. Angella, N.J. Castro, C. Meinert, F.M. Wunner, E. Rank, G. Vozzi, T.J. Klein, I. Catelas, E.M. De-Juan-Pardo, D.W. Hutmacher, Rational design and fabrication of multiphasic soft network composites for tissue engineering articular cartilage: A numerical model-based approach, Chem. Eng. J. 340 (2018) 15–23.
[77] M. de Ruijter, A. Ribeiro, I. Dokter, M. Castilho, J. Malda, Simultaneous Micropatterning of Fibrous Meshes and Bioinks for the Fabrication of Living Tissue Constructs, Adv. Healthc. Mater. 8 (2019) 1800418.
[78] G. Constante, I. Apsite, H. Alkhamis, M. Dulle, M. Schwarzer, A. Caspari, A. Synytska, S. Salehi, L. Ionov, 4D Biofabrication Using a Combination of 3D Printing and Melt-Electrowriting of Shape-Morphing Polymers, ACS Appl. Mater. Interfaces (2021).
[79] D. Nahm, F. Weigl, N. Schaefer, A. Sancho, A. Frank, J. Groll, C. Villmann, H.-W. Schmidt, P.D. Dalton, R. Luxenhofer, A versatile biomaterial ink platform for the melt electrowriting of chemically-crosslinked hydrogels, Mater. Horiz. 7 (2020) 928–933.
[80] N. Dubey, J.A. Ferreira, J. Malda, S.B. Bhaduri, M.C. Bottino, Extracellular Matrix/Amorphous Magnesium Phosphate Bioink for 3D Bioprinting of Craniomaxillofacial Bone Tissue, ACS Appl. Mater. Interfaces. 12 (2020) 23752–23763.
[81] M. Gwiazda, S. Kumar, W. Świeszkowski, S. Ivanovski, C. Vaquette, The effect of melt electrospun writing fiber orientation onto cellular organization and mechanical properties for application in Anterior Cruciate Ligament tissue engineering, J. Mech. Behav. Biomed. Mater. 104 (2020) 103631.
[82] K.F. Eichholz, D.A. Hoey, Mediating human stem cell behaviour via defined fibrous architectures by melt electrospinning writing, Acta Biomater. 75 (2018) 140–151.
[83] M.L. Muerza-Cascante, A. Shokoohmand, K. Khosrotehrani, D. Haylock, P.D. Dalton, D.W. Hutmacher, D. Loessner, Endosteal-like extracellular matrix expression on melt electrospun written scaffolds, Acta Biomater. 52 (2017) 145–158.

[84] E. Bakirci, N. Schaefer, O. Dahri, A. Hrynevich, P. Strissel, R. Strick, P.D. Dalton, C. Villmann, Melt Electrowritten In Vitro Radial Device to Study Cell Growth and Migration, Adv. Biosyst. 4 (2020) 2000077.
[85] B. Delalat, F. Harding, B. Gundsambuu, E.M. De-Juan-Pardo, F.M. Wunner, M.-L. Wille, M. Jasieniak, K.A.L. Malatesta, H.J. Griesser, A. Simula, D.W. Hutmacher, N.H. Voelcker, S.C. Barry, 3D printed lattices as an activation and expansion platform for T cell therapy, Biomaterials 140 (2017) 58–68.
[86] S. Bertlein, D. Hikimoto, G. Hochleitner, J. Hümmer, T. Jungst, M. Matsusaki, M. Akashi, J. Groll, Development of Endothelial Cell Networks in 3D Tissues by Combination of Melt Electrospinning Writing with Cell-Accumulation Technology, Small 14 (2018) 1701521.
[87] I. Pennings, E.E. van Haaften, T. Jungst, J.A. Bulsink, A.J.W.P. Rosenberg, J. Groll, C.V.C. Bouten, N.A. Kurniawan, A.I.P.M. Smits, D. Gawlitta, Layer-specific cell differentiation in bi-layered vascular grafts under flow perfusion, Biofabrication 12 (2019) 015009.
[88] J.G. Baldwin, F. Wagner, L.C. Martine, B.M. Holzapfel, C. Theodoropoulos, O. Bas, F.M. Savi, C. Werner, E.M. De-Juan-Pardo, D.W. Hutmacher, Periosteum tissue engineering in an orthotopic in vivo platform, Biomaterials 121 (2017) 193–204.
[89] D. Janzen, E. Bakirci, A. Wieland, C. Martin, P.D. Dalton, C. Villmann, Cortical Neurons form a Functional Neuronal Network in a 3D Printed Reinforced Matrix, Adv. Healthc. Mater. 9 (2020) 1901630.
[90] L.P. Reynolds, P.P. Borowicz, C. Palmieri, A.T. Grazul-Bilska, Placental Vascular Defects in Compromised Pregnancies: Effects of Assisted Reproductive Technologies and Other Maternal Stressors, in: L. Zhang, C.A. Ducsay (Eds.), Advances in Fetal and Neonatal Physiology, Springer, New York, NY, 2014, pp. 193–204.
[91] T.D. Brown, A. Slotosch, L. Thibaudeau, A. Taubenberger, D. Loessner, C. Vaquette, P.D. Dalton, D.W. Hutmacher, Design and Fabrication of Tubular Scaffolds via Direct Writing in a Melt Electrospinning Mode, Biointerphases 7 (2012) 1–16.
[92] B.L. Farrugia, T.D. Brown, Z. Upton, D.W. Hutmacher, P.D. Dalton, T.R. Dargaville, Dermal fibroblast infiltration of poly($\upepsilon$-caprolactone) scaffolds fabricated by melt electrospinning in a direct writing mode, Biofabrication 5 (2013) 025001.
[93] N. Ristovski, N. Bock, S. Liao, S.K. Powell, J. Ren, G.T.S. Kirby, K.A. Blackwood, M.A. Woodruff, Improved fabrication of melt electrospun tissue engineering scaffolds using direct writing and advanced electric field control, Biointerphases 10 (2015) 011006.
[94] Q. Chen, X. Mei, Z. Shen, D. Wu, Y. Zhao, W. Lingyun, X. Chen, G. He, Z. Yu, K. Fang, D. Sun, Direct write micro/nano optical fibers by near-field melt electrospinning, Opt. Lett. 42 (2017) 5106.
[95] A. Hammerl, C.E. Diaz Cano, E.M. De-Juan-Pardo, M. van Griensven, P.S.P. Poh, A Growth Factor-Free Co-Culture System of Osteoblasts and Peripheral Blood Mononuclear Cells for the Evaluation of the Osteogenesis Potential of Melt–Electrowritten Polycaprolactone Scaffolds, Int. J. Mol. Sci. 20 (2019) 1068.
[96] T. Brückner, A. Fuchs, L. Wistlich, A. Hoess, B. Nies, U. Gbureck, Prefabricated and Self-Setting Cement Laminates, Materials 12 (2019) 834.
[97] S. Bertlein, G. Hochleitner, M. Schmitz, J. Tessmar, M. Raghunath, P.D. Dalton, J. Groll, Permanent Hydrophilization and Generic Bioactivation of Melt Electrowritten Scaffolds, Adv. Healthc. Mater. 8 (2019) 1801544.
[98] N.C. Paxton, J. Ren, M.J. Ainsworth, A.K. Solanki, J.R. Jones, M.C. Allenby, M.M. Stevens, M.A. Woodruff, Rheological Characterization of Biomaterials Directs Additive Manufacturing of Strontium-Substituted Bioactive Glass/Polycaprolactone Microfibers, Macromol. Rapid Commun. 40 (2019) 1900019.
[99] F. Tourlomousis, C. Jia, T. Karydis, A. Mershin, H. Wang, D.M. Kalyon, R.C. Chang, Machine learning metrology of cell confinement in melt electrowritten three-dimensional biomaterial substrates, Microsyst. Nanoeng. 5 (2019) 1–19.
[100] E. Hewitt, S. Mros, M. McConnell, J.D. Cabral, A. Ali, Melt-electrowriting with novel milk protein/PCL biomaterials for skin regeneration, Biomed. Mater. 14 (2019) 055013.